MICROSTRUCTURE AND PROPERTIES OF COPPER THIN FILMS ON SILICON SUBSTRATES

A Thesis

by

VIBHOR VINODKUMAR JAIN

Submitted to the Office of Graduate Studies of
Texas A&M University
in partial fulfillment of the requirements for the degree of

MASTER OF SCIENCE

August 2007

Major Subject: Mechanical Engineering

MICROSTRUCTURE AND PROPERTIES OF COPPER THIN FILMS ON SILICON SUBSTRATES

A Thesis

by

VIBHOR VINODKUMAR JAIN

Submitted to the Office of Graduate Studies of
Texas A&M University
in partial fulfillment of the requirements for the degree of

MASTER OF SCIENCE

Approved by:

Chair of Committee, Xinghang Zhang
Committee Member, Karl Hartwig
Haiyan Wang
Head of Department, Dennis O'Neal

August 2007

Major Subject: Mechanical Engineering

ABSTRACT

Microstructure and Properties of Copper Thin Films on Silicon Substrates

(August 2007)

Vibhor Vinodkumar Jain, B.E., Shivaji University, India

Chair of Advisory Committee: Dr. Xinghang Zhang

Copper has become the metal of choice for metallization, owing to its high electrical and thermal conductivity, relatively higher melting temperature and correspondingly lower rate of diffusivity. Most of the current studies can get high strength copper thin films but on an expense of conductivity. This study proposes a technique to deposit high strength and high conductivity copper thin films on different silicon substrates at room temperature. Single crystal Cu (100) and Cu (111) have been grown on Si (100) and Si (110) substrates, respectively. Single crystal Cu (111) films have a high density of growth twins, oriented parallel to the substrate surface due to low twin boundary energy and a high deposition rate. The yield strengths of these twinned Cu films are much higher than that of bulk copper, with an electrical resistivity value close to that of bulk copper. X-ray diffraction, transmission electron microscopy and nanoindentation techniques were used to show that high density twins are sole reason for the increase in hardness of these thin films. The formation of growth twins and their roles in enhancing the mechanical strength of Cu films while maintaining low resistivity are discussed.

To my Parents and my little Sister

ACKNOWLEDGEMENTS

Behind every achievement that we see in this world today are unseen hands of many. Similarly in my diligent endeavor to carry out this work I was fortunate enough to have support from a large number of people to whom I owe many things. I take this opportunity and with full respect fully acknowledge them all for fueling my aspiration through their consistent support and cooperation.

I express my deep sense of gratitude to my advisor and source of enlightment, Dr. Xinghang Zhang and my committee members Dr. Karl Hartwig and Dr. Haiyan Wang, for they were instrumental in guiding me to my desired destination.

I thank the incorrigible optimists in Doherty 314, Engang Fu, Osman Anderoglu, Nan Li and David Foley, for their helpful cooperation, advice and assistance with my work. Words are indeed not enough to thank my friends, Abhinav Kumar, Vivek Cherian, Gaurang Sarvaiya, Nimish Seth, Sethu Madhukar, Kiran Shakhardande, Meetu Swaroop, Suhani Shah, Dipin Sahaney, Sweety Shah and Jigyasa Desai, for their constant motivation and encouragement.

The word ‘thanks’ itself falls short with respect to the person without whom I wouldn’t have seen the light of day. Herein I extend my gratitude to my beloved father, Dr. Vinod Kumar Jain, for his staunch support, his invaluable guidance and above all faith in me. My mother, Suman Jain and sister Surabhi Jain, taught me to stand on my own feet and I thank them for their enduring support and timely cooperation. Thanks to all my friends and well wishers and peer group for making me believe in myself.

TABLE OF CONTENTS

Page

LIST OF FIGURES

FIGURE Page

FIGURE Page

FIGURE Page

FIGURE Page

FIGURE Page

LIST OF TABLES

TABLE Page

1. INTRODUCTION

Recently copper has become a primary focus for the integrated circuit metallization replacing aluminum owing to its higher electrical and thermal conductivity, higher melting temperature and correspondingly lower rates of diffusivity. These advantages have drawn significant research in the areas of deposition, characterization and copper films and enhancement of film quality via tailoring deposition techniques. As conducting materials are being used in many diverse applications, it is required that they have both high strength and conductivity at the same time. However, pure metals for example silver, copper and aluminum are very soft. Strengthening these metallic films by various approaches like grain size reduction, solid solution strengthening, cold working leads to high strengths but low electrical conductivity. For instance Cu with 2 or 3 time higher strength (achieved by alloying), usually has a loss of conductivity about 50 to 60 percent in comparison with pure copper. The primary source of strengthening of thin films has been confining dislocation motion. Introduction of defects, such as grain boundaries and precipitates, have proven to be an effective technique to enhance mechanical strengths to a great extent. But these defects also act as a very powerful scattering site for electrons, and thus lead to a lower electrical conductivity. Such dilemma has led to exploration of a different type of defects, twin boundaries. Twin boundaries act as barriers to dislocation motion in a similar manner to grain boundaries, but the electrical scattering coefficient at coherent twin boundaries is about one order of magnitude lower than that at grain boundaries.

This thesis follows the style and format of Scripta Materialia.

Therefore there is great potential in design high-strength and high-conductivity Cu films by tailing twin boundaries. The primary goal of present work is to deposit copper, single crystal in nature with good balance of electrical and mechanical properties.

1.1. Thin film deposition

Thin films can be defined as "thin material layers ranging from fractions of a nanometer to several micrometers in thickness" [1]. A proper distinction between thin film deposition and thick film deposition should be bared in mind. Thin film deposition involves deposition of individual atoms, while the latter deals with the deposition of particles, for example thick film technique is painting [2]. Usually thick film deposition doesn't give much control over the quality of films and is relatively inexpensive than thin film deposition. Today thin film technology itself is a separate branch of material science and has evolved into a set of techniques used to fabricate many products [3]. Applications include very large scale production of electronic packaging, sensors, integrated circuits, optical film and devices and also protective and decorative coatings. At present, the enormous opportunities and rapidly changing needs for thin films and thin film devices are opening new frontiers for the development of new processes, materials and technologies [4, 5, and 6].

1.1.1. Thin film deposition steps

Almost all thin film deposition techniques have four or five basic sequential steps as shown in Fig. 1. A source of pure material to be deposited acting as a target in growth process, such as in physical vapor deposition. Material is transported to the substrate via

either liquid or vacuum medium. The deposition of the material onto the substrate then follows; this process may or may not be followed by annealing process depending on the desired properties of the thin film to be deposited. In final step the film is analyzed to evaluate the process. And the analysis is incorporated in order to adjust the deposition conditions.

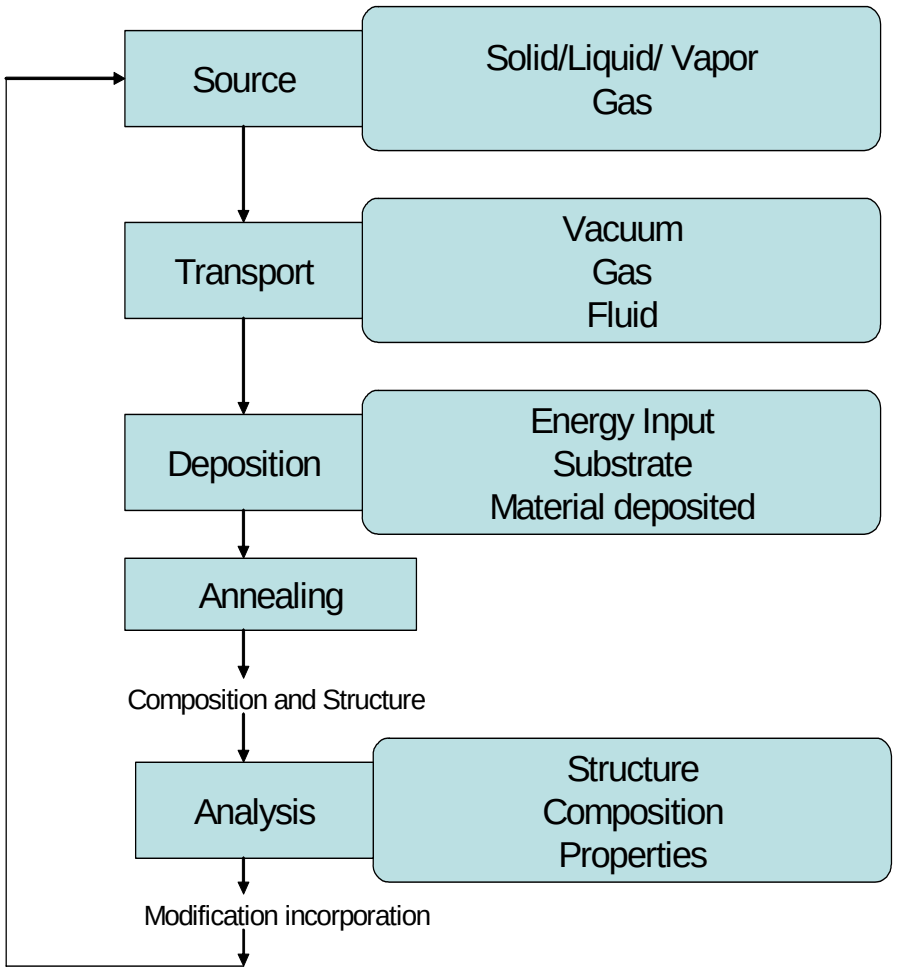

Figure 1 Schematic repesentation of thin film deposition steps

A source of material for thin film deposition may be a solid, liquid, vapor or gas. For solid materials we need to device a method to vaporize them and transport them to the substrate. Various known methods to do this are to heat the target, hit it with high energy ions, laser beam or electron beam. These methods are appropriately called Physical vapor deposition (PVD). In many cases the material is supplied in the forms of gases or liquid and deposition occurs right after chemical reaction close to substrate. Such growth process is typically called chemical vapor deposition (CVD). In both CVD and PVD techniques impurity contamination and supply rate are major areas of interest. The thin film properties are dependant on the deposition rate and the amount of materials supplied and thus the deposition rate is of importance.

Uniformity or arrival rate over the substrate is the major area of concern in transport step. Uniformity of the thin film deposited is dependent on the type of deposition process CVD or PVD. Basically, the atoms travel in straight path in high vacuum system during PVD process with little or negligible amount of collision, whereas in CVD process, they have random paths with lots of collisions due to the usage of chemical gasses or liquid.. Thus, the uniformity in the case of vacuum system is dependent on the supply rate and the geometry of the substrate surface. Whereas, in a CVD process the uniformity is dependent on the gas or liquid flow patterns and on the diffusion of the source molecules through the surrounding other gases involved. There is an added advantage with High vacuum transport medium i.e. the clear access to the deposition surface; this allows the possible use of the analytical techniques involving electron beams.

Often termed as heart of thin film deposition process, deposition step is considered to be composed of six different sub sequences. The atoms and molecules arriving encounter **absorption.** Upon arrival near the surface, molecules or atoms feel an attraction due to interaction with the surface molecules. This happens even in symmetrical molecules or atoms as they also behave as oscillating dipoles and causes induced dipole interaction called Van der Waal's force. The absorbing species then go though **surface diffusion** to find most active sites or find epitaxial sites. This process requires breaking bonds between the absorbate and the surface site so that the absorbate can move to new location and form new bonds.

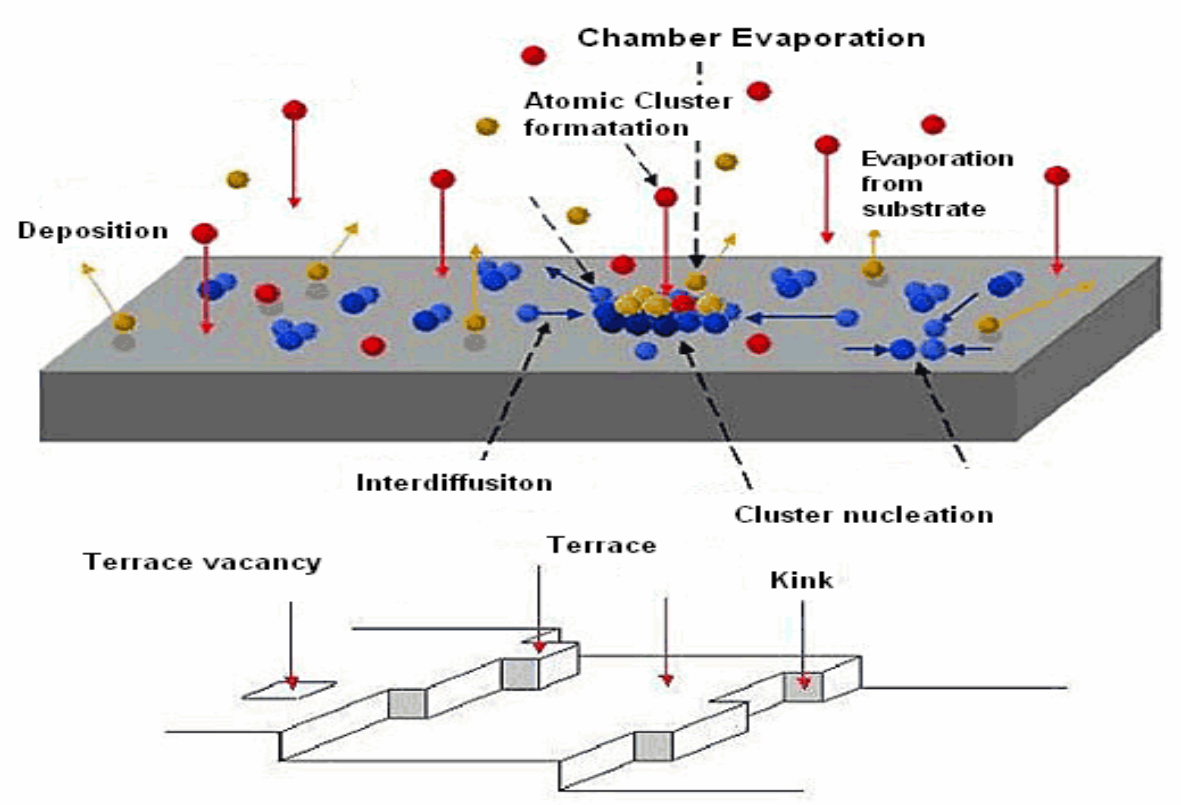

Figure 2 Atom/molecule interactions with substrate [7]

In the process of surface diffusion the atoms or molecules interact within themselves and form bigger clusters (See figure 2). These clusters or nuclei are thermodynamically unstable and tend to desorb in time depending on the deposition parameters. After reaching a certain size the clusters becomes thermodynamically stable and the nucleation barrier is said to have been overcome. This step involving the formation of stable, critical sized nuclei is called the nucleation stage [2].

The critical nuclei grow in number as well as in size until a saturation nucleation density is reached. The nucleation density and the average nucleus size depends on a number of parameters such as the energy of the impinging species, the rate of impingement, the activation energies of adsorption, desorption, thermal diffusion, temperature, topography, and chemical nature of the substrate. A nucleus can grow both parallel to the substrate by surface diffusion of the adsorbed species, and perpendicular to it by direct impingement of the incident species. In general, however, the rate of lateral growth at this stage is much higher than the perpendicular growth. The grown nuclei are called islands.

In coalescence stage, small islands start coalescing with each other in an attempt to reduce the substrate surface area. This tendency to form bigger islands is termed agglomeration and is enhanced by increasing the surface mobility of the adsorbed species, for example increasing the substrate temperature. In some cases, formation of new nuclei may occur on areas freshly exposed as a consequence of coalescence. Larger islands grow together, leaving channels and holes of uncovered substrate. The structure

of the films at this stage changes from discontinuous island type to porous network type. Filling of the channels and holes forms a completely continuous film [7].

1.2. Thin film deposition techniques

Rapidly changing needs for the thin film materials and devices are creating new opportunities for the development of the new processes, materials and technologies. There are basically three categories of thin film deposition processes: PVD, CVD and chemical methods (Figure 3). It should be noted here that it is improper to associate high vacuum to categorize these processes as both PVD and some of the CVD processes use high vacuum environment [8].

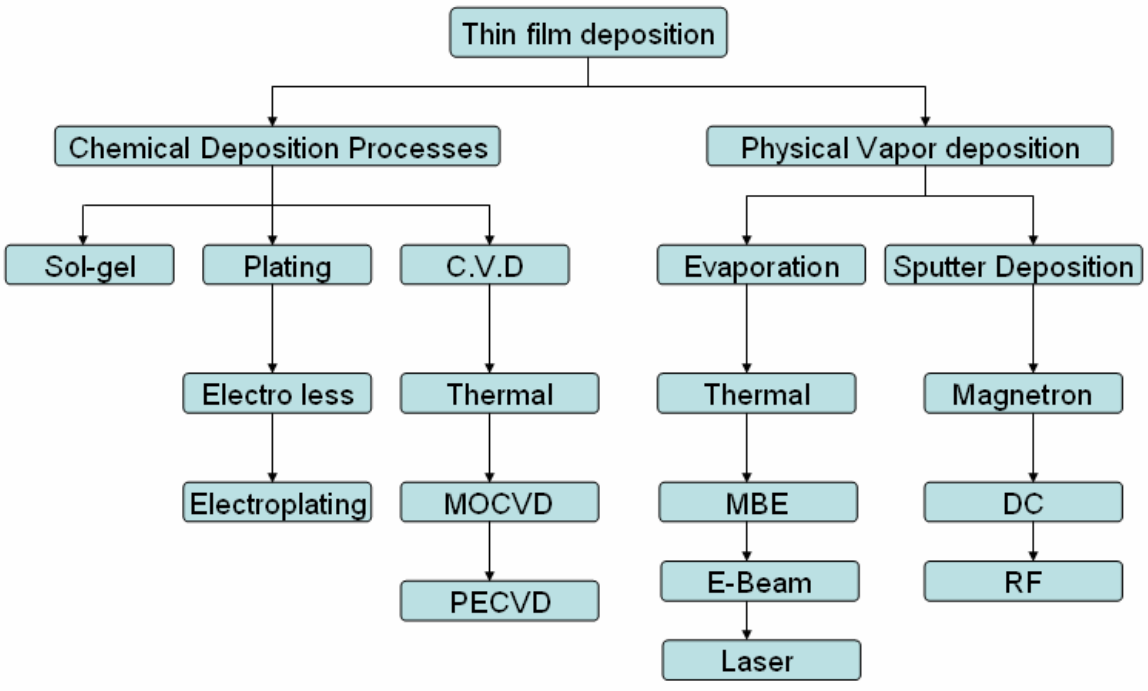

Figure 3 Thin film deposition techniques

1.2.1. Physical vapor deposition

Physical vapor deposition is an atomistic deposition process, where materials are transported in the form of vapor to the substrate where it condenses, in the presence of high vacuum or low pressure. These processes can be used to deposit thin film ranging form few nanometers to thousands of nanometers, however they can also be used to form multilayer coating, graded composition deposits, very thick deposits and freestanding structures. Substrate can range from very small to very large sizes and from flats surfaces to complex geometries [9].

PVD processes can be used to deposit films of elements and alloys as well as compounds using reactive deposition processes. In reactive deposition processes, compounds using reactive material with the ambient gas environment such as nitrogen are employed. Quasi-reactive deposition is the deposition of films of a compound material from a compound source where loss of the more volatile species or less reactive species during the transport and condensation process, is compensated for by having a partial pressure of reactive gas in the deposition environment [9, 10].

The PVD process is divided into two major categories: Sputtering and thermal evaporation.

1.2.2. Sputter deposition

Sputtering is an important PVD technique, when a solid surface is bombarded with energetic particles such as accelerated ions, surface atoms of the solid are scattered backward due to collisions between the surface atoms and the energetic particles. This phenomenon is called as back sputtering or just sputtering. Cathode sputtering is used

for the deposition of thin films. Several sputtering systems are proposed for thin film deposition including dc diode, rf diode, magnetron, and ion beam sputtering. The dc sputtering system is composed of a pair of planar electrodes. One of the electrodes is a cold cathode and the other is the anode. The front surface of the cathode is covered with target material to be deposited. The substrates are placed on the anode. The sputtering chamber is filled with sputtering gas, typically argon gas. The glow discharge is maintained under the application of dc voltage between the electrodes. The positive argon ions generated in the glow discharge are accelerated at the cathode fall and sputter the target, resulting in the deposition of the thin films on the substrates as seen in figure 4.

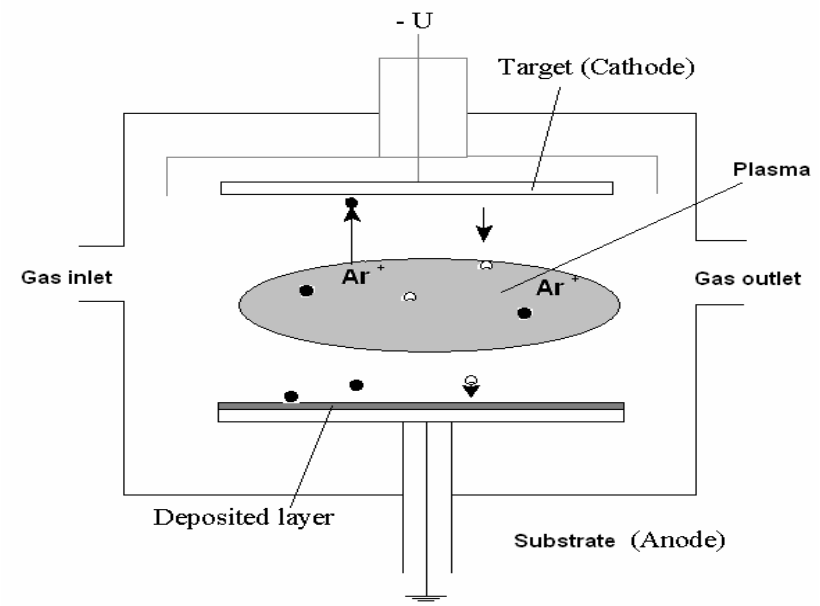

Figure 4 Schematic representation of sputter deposition system [11]

In order to sustain the glow discharge with insulator target, rf voltage is supplied to the target. Hence, the system is called rf sputtering system. In magnetron sputtering, a parallel magnetic field is superposed on the glow discharge. Electrons in the glow discharge show cycloid motion, and the orbit drifts in the direction of the E × M, Where E and M denote the electric field in the discharge and the superposed magnetic field. Magnetic field is oriented such that these drift paths for electrons form a closed loop. This causes an increased rate of collision between the electrons and the sputtering gas molecules. The magnetic field causes the plasma density to increase which leads to increased current density at the cathode and hence causing to increase the sputtering rate and efficiency of the sputtering reactor [10, 11].

1.2.3. Thermal evaporation

Thermal evaporation deals with the evaporation of the source materials in a vacuum chamber and condensing the evaporated particles on a substrate. This process is conventionally called vacuum deposition. Besides regular thermal evaporation and e-beam evaporation, molecular beam epitaxy (MBE) is one of the most reliable deposition processes in thermal evaporation (See figure 5). The system is a controlled process, where the evaporation rate of the source materials is controlled in situ by a computerized process control unit. This kind of deposition process is now widely used for the controlled deposition of alloys and compounds. A typical MBE system is composed of a growth chamber, the analysis chamber and, a sample chamber [10].

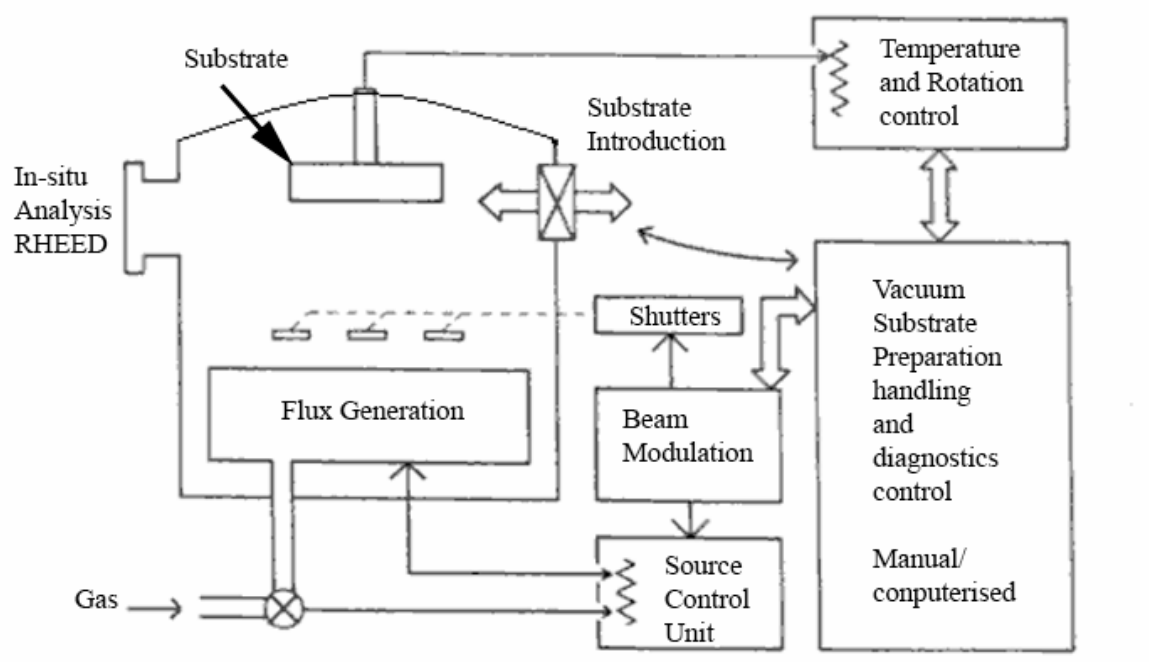

Figure 5 Schematic representation of molecular beam epitaxy system [10]

1.2.4. Pulsed laser deposition

(PLD) is an improved thermal process used for the deposition of alloys and compounds with a controlled chemical composition. In this process a high power pulsed laser is irradiated onto the target of source materials through a quartz window. Laser power density is increased by a use of quartz lens. The target material is locally heated by this high density laser and causes the target material to melt and vaporize in vacuum, atoms vaporized get collected on nearby sample surfaces to form thin films (See figure 6). PLD is simple in design and has an advantage of target being of different forms such as powder, sintered pellet, and single crystal [11].

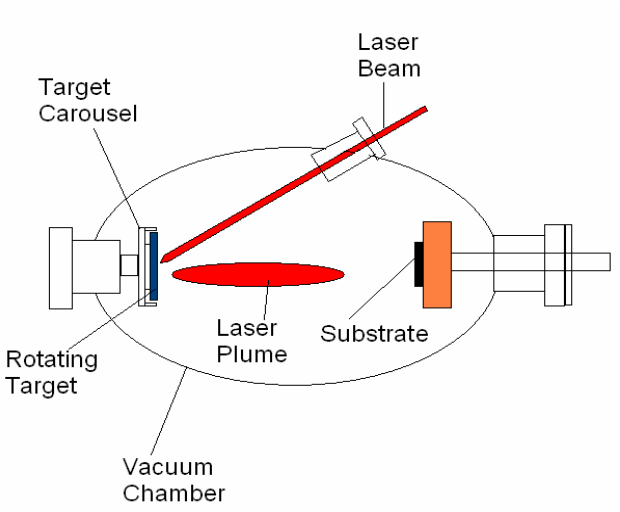

Figure 6 Schematic diagram of pulsed laser deposition system [11]

1.2.5. Chemical vapor deposition

In chemical vapor deposition one or more gaseous species are used to react with/on a solid surface and one of the reaction products is a solid phase material. Some of the basic steps involved in a CVD process are enlisted as follows [12] (See figure 7):

1. Transport of reactants by forced convection to deposition region.
2. Transport of reactants by diffusion from the main gas stream through the boundary layer to the wafer surface.
3. Adsorption of reactants on the wafer surface.
4. Surface processes, including chemical deposition or reaction, surface migration to attachment sites, site incorporation and other surface reactions.
5. Desorption of byproducts from the surface.

6. Transport of byproducts by diffusion through the boundary layer and back to the main gas stream.
7. Transport of byproducts by forced convection away from the deposition region.

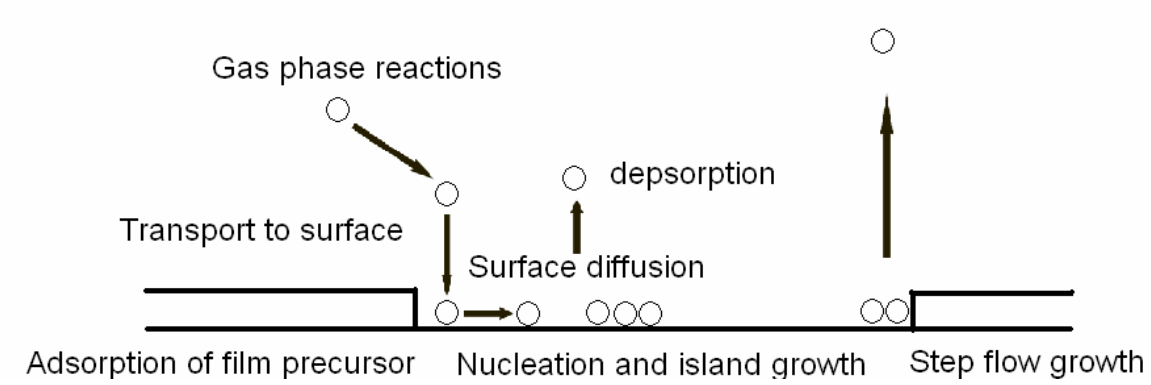

Figure 7 Schematic representation of chemical vapor deposition process [11]

1.3. Microstructure of epitaxially grown Cu thin film

Recently, copper has come in lime light of researcher due its future in electronic packaging applications. Copper has become the conductor of choice owing to its low electrical resistivity i.e. 1.67μΩcm which is less than aluminum 2.65 μΩcm, and large electro-migration resistance, it is also a favorite area of research due to the potential application in metallization of semiconductor devises such as ULSI [13,14]. An immense effort is being dedicated to deposit high quality thin film copper by various techniques.

Evaporation deposition process is a classical way of depositing thin film and is relatively simple. Thermal Evaporation deposition is a very economical way depositing thin films but the quality of films and microstructure obtained by evaporation depositions has always been a sight of concern for evaporation deposition, Jian and Mayer stated that in 80nm thick copper deposited by e-beam evaporation on NaCl and SiO_2 at a vacuum of 2×10^{-7}Torr showed traces of non-uniform deposits and microstructural defects when observed in transmission electron microscopy. TEM images revealed the presence of randomly distributed 0.5μm grains. The film was then annealed for one hour at 300°C after which normal grains grew to 50nm but still there was no significant growth in secondary grains [15]. Thermal Evaporation deposited thin films do not show good chemical bond with the substrate due to the low kinetic energy and have non uniformity in sticking coefficient [16]. MBE is a new development in evaporation process and facilitates the deposition of high quality thin films by slow evaporation of material from Knudsen effusion cells; the deposition process is controlled

very accurately by a computerized system [17]. MBE is very expensive technique of depositing and is certainly not suitable for mass depositions.

High quality thin film can be grown by dc magnetron sputtering of high purity copper target in a high vacuum environment [18]. Kah Yoong Chan and group [19] deposited Cu with strong (111) texture on P-type silicon by dc magnetron sputtering system, a 5.08cm diameter circular target of purity 99.995% purity. The argon used was 99.995% pure and the substrate used was 6mm ×12mm in dimensions and the deposition was done at room temperature. It was seen that the higher deposition power increased the Ar ion flux and kinetic energy leading to better sputtering of atoms and energy for movement on surface of substrate. The film obtained is also continues and high quality with less voids, the diffusion of adatoms, and moment transfer to the film was enhanced this led to higher diffusion lengths, which led to settlement of adatoms in voids and in turn deposition of continues and high quality film. All the measurements in these experiments were done by AFM, X-ray diffraction showed dominant presence of Cu (111) and traces of Cu (100) oriented grains.

1.3.1. Intermixing of copper and silicon

As seen from the literature survey and above examples substrate heating and post deposition annealing is integral part of evaporation processes in order to get high quality films. In the copper silicon system this leads to formation of silicides which could range up to 200nm thick. The atomic mixing and formation of silicides during deposition of a thin film are caused by diffusion processes which are dominated by thermal effects (See figure 8) and are also influenced by the energy of the incident particles [20]. The two

main reasons for interface mixing in Cu and Si is solid state chemical reaction at interface and increase in diffusivity. The diffusion of copper into silicon increases in an order of magnitude as the temperature increases above 120°C (See figure 8). Better quality deposits can be obtained at lower substrate temperatures by sputter depositions, thus large scale interdiffusion can be avoided. The secondary electrons generated at the target in magnetron sputtering do not hit the substrates as they are confined in the cycloidal trajectories near the target and so do not cause the increase in temperature of substrate, enabling the use of low temperature substrates and surface sensitive substrates. Even though there is less interdiffusion the film formed adheres to the substrate due to localized mixing caused by the high kinetic energy impacts. MBE (requires UHV) and electroplating can be used to produce high quality films but complexity and cost of the process are the limiting factor. On the other hand in magnetron sputtering ions have higher kinetic energy which leads to higher deposition rates and better deposition conditions as the adatoms have higher interdiffusion lengths thus the films obtained are of better quality [21, 17].

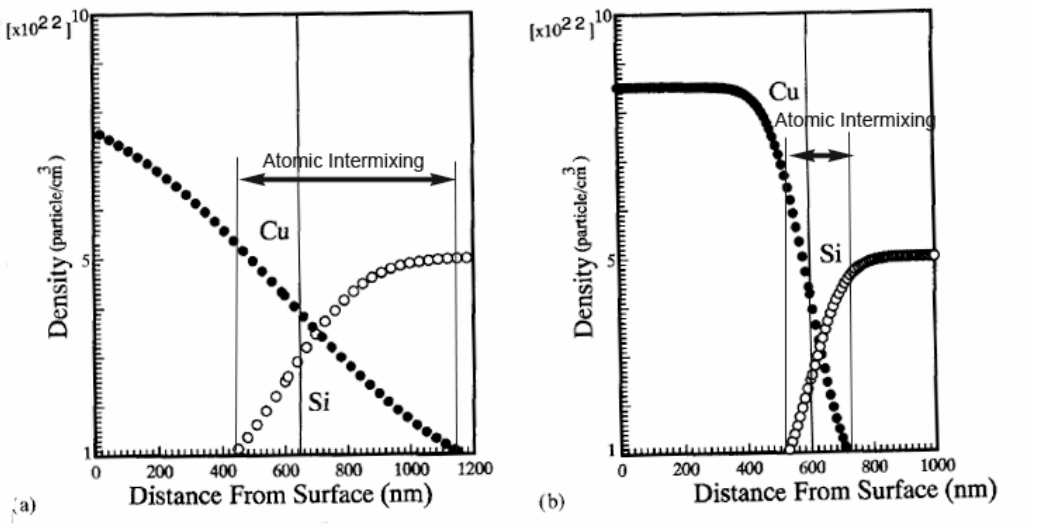

Figure 8(a) Interatomic mixing of copper and silicon at 300°C. (b) Interatomic mixing of copper and silicon at 100°C

1.3.2. Single crystal copper

A mono-crystal or single crystal solid is a type of solid in which the crystal lattice orientation is continuous and unbroken to the edges of the sample, i.e. the sample is free from grain boundaries. Grain boundaries have significant effects on various properties of a material, and can have effects on the functionality of the material which are eliminated in the case of single crystal copper [22].

1.3.2.1. Epitaxial growth of single crystal copper thin film

Many research groups have dedicatedly worked on various methods to grow single crystal copper films, some of these novel methods are explained briefly below.

Single crystal Cu with (111) orientation was grown on mica surface by M.A Otooni in 1978 (See figures 9 and 10) [23]; this process took the advantage of seeding effect to enhance the continuity of the thin films. Seeding the surface with nuclei

induced two different effects: 1) the nuclei acted as new source for the supply of copper atoms to the thin regions of the film; 2) At the nuclei edges thin regions could be produced due to the lateral growth of nuclei. The seeding areas had four five carbon coated grids on freshly cleaved mica substrate. The evaporated metal passes through the grid and formed the desired seeds and deposited copper nuclei of approximately 700-800 A° thickness. The substrate during this process was at 435°C and at a vacuum of 2 $\times 10^{-6}$ Torr and the sample was annealed for 4hours before gradual cooling at the room temperature. Now, the grid is removed and is followed by second phase of deposition in which a layer of copper of thickness 200-300A is deposited at a substrate heated at 435°C and at a vacuum of 2×10^{-6} Torr. [23]

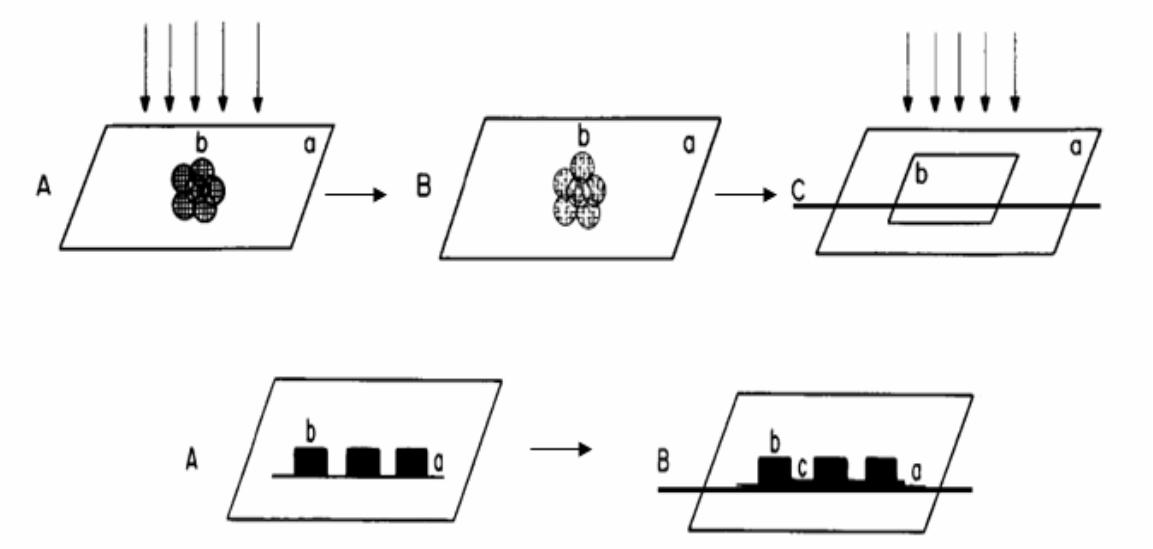

Figure 9 Schematic representation of the deposition process: 1) Evaporation on the grid, 2) Removal of the grid, and 3) Deposition on the mica

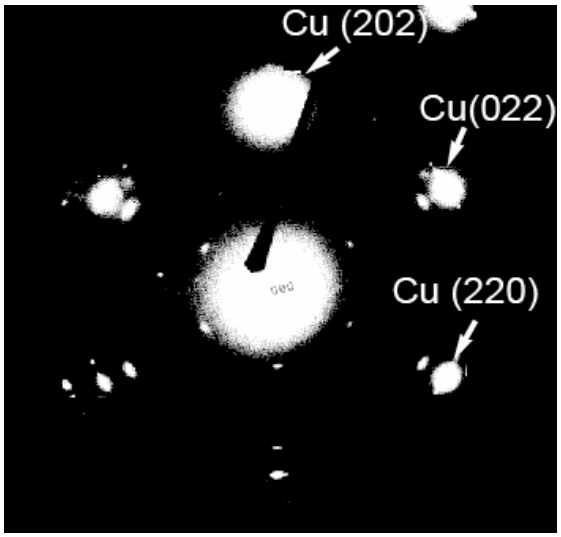

Figure 10 TEM diffraction pattern for Cu (111) as obtained by deposition over mica substrate

Copper was also deposited using a dc magnetron sputtering with a base pressure of 1.3×10^{-7}Pa on Magnesium oxide substrate by J.M. Purswani and group. The substrates were polished and cleaned with repeated bath of trichloroethylene, acetone, isopropanol, and deionized water then dried using dry N_2.

The substrate was then thermally degassed at 800°C for 1 h. A water cooled copper target was used to as a source and was at a distance of 25cm. The target was first cleaned for first 5mins with the substrate covered to protect it from any unwanted deposition. Sputtering was then carried out at 150W power, giving a deposition rate of 10nm/sec. After deposition the substrate was let cool to a temperature of 50°C, several deposition were done at different deposition temperatures of 50,100, 200°C and the epitaxial orientation was determined using X-ray diffraction and was found that the copper film deposited to be single crystal copper of (100) [24] (See table 1).

Brockway and Marcus [25] worked on single crystal copper thin film; they deposited single crystal copper film on to NaCl substrate. These single crystal copper films were deposited by physical vapor deposition of 99.999% pure copper at a rate of 400 A/min. The NaCl surface was polished with moist metallographic polishing cloth and rinsing in methanol. NaCl was maintained at a temperature of 330°C during condensation process and then cooled to room temp in about 7-8 mins. The condensed films were annealed at a temperature of 630°C for approximately ten minutes [25] (See table 1).

Table 1
A systematic representation of various techniques for epitaxial growth of Cu [24, 25, 26-32]

Deposition Technique	**Substrate**	**Temp**	**Buffer Layer**	**Growth rate**	**Cleaning Technique**	**Vacuum**
Thermal Evaporation	Cleaved Mica Monoclinic	425°C	Not Known	Not Known	Not Known	2×10^{-6}Torr
Thermal Evaporation	NaCl F.C.C a=5.62 Å	300°C	Not Known	Not Known	Not Known	2×10^{-7}Torr
Thermal Evaporation	NaCl F.C.C a=5.62 Å	330°C	Not Known	400A /min	Polishing-water and methanol bath	10^{-5} Torr
Thermal Evaporation	c-cut Sapphire Trigonal	200-630°C	Not Known	0.2-2nm/s	Super-Polishing, rinsing in alcohol and glow discharge (argon)	5×10^{-6}Torr
Thermal Evaporation	NaCl F.C.C a=5.62 Å	325°C	Not Known	Not Known	Cleaved NaCl	10^{-7}Torr
Magnetron Sputtering	Silicon D.C.S a=5.392 Å	Not Known	Not Known	0.4-0.88nm/s	Etched with 10% HF solution	4×10^{-5} Pa
Thermal Evaporation	NaCl-F.C.C / Mica-Monoclinic	440°C	Not Known	11-14A/s	Not Known	5×10^{-9}Torr
Sputtering	Silicon D.C.S a=5.392 Å	777-877°C	Molybdenum B.C.C	10A /min	Not Known	10^{-10}Torr
e-beam Evaporation	Silicon D.C.S a=5.392 Å	Not Known	No Buffer layer	Not Known	Etched in 1:50 HF:H_20 Annealed for 10 min at 850°C	10^{-10}Torr

1.4. Mechanical properties

Improved mechanical properties of metals, has always remained of key area of interest of metallurgist and material science engineers. There are several hardness enhancement techniques are available and the one to be applied depends on the properties required and its ability to tailor it. Usually hardness of a metal is improved by a little sacrifice of ductility [22].

Hardness is defined as the ability of a material to resist deformation. Deformation on the other hand corresponds to large number of dislocation motions, many dislocation in crystalline metals are edge and screw dislocations [33, 34]. For this reason practically all strengthening mechanisms of materials eye towards restraining and hindering the motions of dislocations. Some of the well known phenomenons for strengthening are reduction of grain size, solid-solution strengthening, and strain hardening.

1.4.1. Grain-size reduction

An immense amount of concentration is being paid in the contemporary time towards grain-size reduction induced hardness in metals. Grain boundaries have proved to be a strong barrier to the motion of dislocation. This is because different gains in neighborhood have different orientations, so in order to cross the grain boundary the dislocation motion has to change the direction of motion and with in a grain boundary region due to atomic disorder there is discontinuity of slip planes from one grain to another. As the grain size decreases the harder the metal gets this phenomenon is governed by 'Hall-Petch equation'

$$\sigma_y = \sigma_0 + k_y d^{-1/2} \quad (1)$$

where σ_y is yield stress, d is the average grain diameter; σ_0 minimum stress needed to cause a dislocation motion (material constant) and k_y is fitting parameter and is constant for a material [24-26, 35-37].

In nanocrystals due to presence and influence of defects such as porosity, dislocation many authors have posted observation of what is called as inverse Hall-Petch relationship, i.e. the softening of materials occur with decreasing the grain size after an extent. According to this theory at nano-level the deformation process is different than the traditional way, the deformation is no longer dominated by dislocation motion but are now dependent on the grain boundary sliding and as the grain boundary become smaller more the sliding will cause the material to become soft [38-41].

1.4.2. Solid-solution strengthening

One of the most commonly seen strengthening mechanism in metals is adding impurity atoms to form substitutional or interstitial solid solution, in other word to alloying the metal, This is called as solid-solution strengthening. Almost all high purity metals are seen to be softer and weaker than their alloys with same base metal. The concentration of these impurities shows an increase in tensile and yield strength.

The impurity atoms (solute) take place in between the pure metal (solvent) atoms and impose strain onto the neighboring atoms. This imposed strain interacts with the dislocations and restrict their motions causing hardening of metal. When solute and solvent atoms differ in size, local stress fields are created (if solute atom size is larger than solvent atom size, this field is compressive, and similarly, when solute atoms are smaller than solvent atoms, this field is tensile). Depending on their relative locations,

solute atoms will either attract or repel dislocations in their vicinity, requiring a higher force to overcome the obstacle. This is known as the **size effect**. In substitutional solid solutions, these stress fields are spherically symmetric, meaning they have no shear stress component. As such, substitutional solute atoms do not interact with the shear stress field characteristic of screw dislocations. Conversely, in interstitial solid solutions, solute atoms cause a tetragonal distortion, generating a shear field that can interact with both edge, screw, and mixed dislocations [42, 22].

1.4.3. Cold working

Cold working means working of metals below their recrystallization temperature. Due to cold working the hardness increases on the expense of ductility. Basically cold working leads to strain hardening due to multiplications of dislocation, an anneal metal contains about 10^4-10^6 dislocations per mm^2 while a cold worked metal may have about 10^{11} dislocations per mm^2.

During initial stages of plastic deformation the dislocations form a coplanar array, as this deformation continues cross slip takes place and multiplication of dislocation is seen, on further deformations high dislocation density or tangles formation is seen, which then enhances to tangling network. Most of the energy exhausted during deformation is in the form of thermal energy but some part of it is used to increase the internal energy of the system by being stored in the crystal lattice [43].

1.4.4. Strengthening of thin films

Strengthening of thin films act in a very different manner than in bulk material, for example in thin films of nanometer regime solid solution hardening is not an option as the impurities tend to diffuse to the grain boundary region. For example in electrodeposited nanocrystalline nickel, carbon impurities tend to diffuse in side the grain boundary. On the other hand the hindering the dislocation motion still is the main objective of most of the hardening techniques in thin films and so hall petch relation still holds true for thin films [44]

1.4.5. Grain-size reduction in thin film

Grain size reduction works is a similar fashion as it works in bulk materials and thin film have been seen with increasing hardness as the grain size go smaller, following the hall-petch equation. M.D Merz and group deposited copper films with grain size ranging from 8 to 0.056μm, these films showed an increasing trend in yield strength from 73.4 to 481 MPa confirming hall-petch relation ship [45]. Based on this relationship nanocrystalline materials are expected to show higher strengths than microcrystalline material. Nanocrystalline copper was deposited by means of magnetron sputtering process also two other batch one with surface mechanical attrition treatment (SMAT) and ECAE process were made the average grain size was 2 to 18mn for the former and 10nm for the later, the hardness values obtained are 3.02 GPa for the former and 1.75 and 1.67 GPa for the later and concluded that 10nm small grain size copper also follow hall-petch relation [46, 35]. A schematic graph showing grain size strengthening in different system is shown below in figure 11 [47-50].

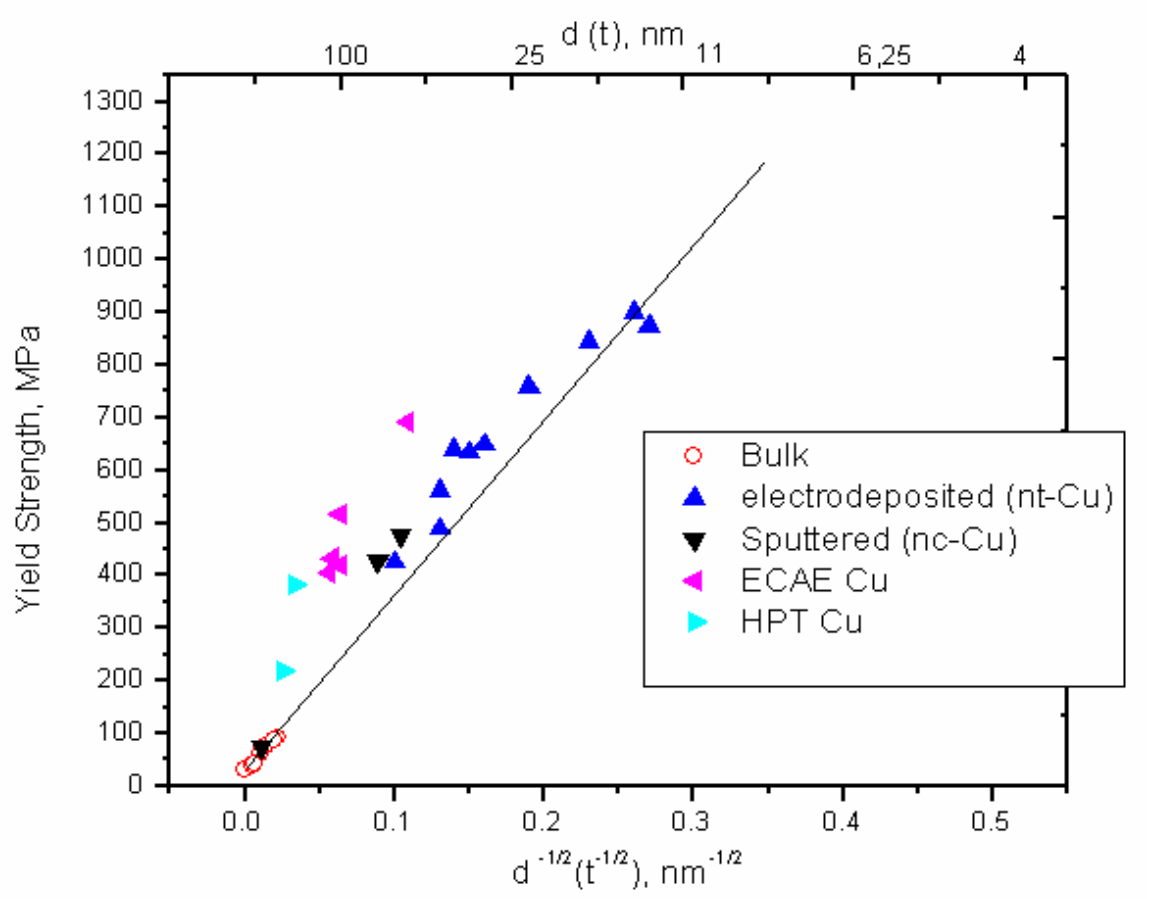

Figure 11 Plot of yield strength vs. grain diameter (d^{-1})

1.4.6. Film thickness reduction

It is known that the thin film materials show more strength than their bulk counter parts; this high strength is attributed to the microstructure of these thin films. It has been seen that the grain size in thin film materials usually don't increase more that the film thickness and so inherently thin films are stronger owing to small grain size [51, 52]. Apart from the grain size the dislocation density of a thin film is usually higher that bulk materials, this is due to the misfit stresses generated in the thin film deposited over thick substrate, to relax these stresses threading dislocations are formed which contribute to

high dislocation densities. Dislocation motions in thin films are also hindered by the substrate and the oxide layer, if present.

$$\sigma = \frac{\sin\Phi}{\cos\Phi\cos\lambda}\frac{b}{2\pi(1-v)h}\left[\frac{\mu_f\mu_s}{\mu_f+\mu_s}\ln\left(\frac{\beta_s h}{b}\right)+\frac{\mu_f\mu_o}{\mu_f+\mu_o}\ln\left(\frac{\beta_o t}{b}\right)\right] \quad (2)$$

where $\mu_f\,\mu_s$ and μ_o are elastic shear moduli of film, substrate and oxide,Φ and λ are angle between glide plane normal and film normal, film normal and burgers vector, h is the thickness of film, t is the thickness of oxide, β_s and β_o are numerical constants i.e. 2.6 and 17.5

The above expression predicts the increase in yield strength increase in thickness, but it doesn't take into account the increase in the strength due to other factors such as point defects, grain boundary etc [53, 54]

1.5 Electrical resistivity

Quantum mechanics says that there should not be any interaction between accelerating electrons and atoms in a perfect crystal lattice, which implies that there should be a continues increase in current with time as long as the electric field is applies. In practicality this in not true and the current reaches a constant value, which suggests that there must be some resistance to flow of electrons. This could be scattering due to dislocations, grain boundaries or thermal vibrations etc [22, 55].

In metals scattering of electrons are affected by defects in the crystal lattice, as the number of these defects increase there is increase in the resistivity of the metals. It is said that the total resistivity of the metal is the sum of resistivity contribution by thermal vibrations, impurities and plastic deformation.i.e.

$$\rho_{total} = \rho_t + \rho_i + \rho_d \qquad (3)$$

1.5.1.Temperature influence

As the temperature rises there is an increase in the thermal vibrations and lattice irregularities, these vibrations and irregularities act as electron scattering centers and so it is observed that there is an increase in resistivity as the temperature increases above -200°C.

$$\rho_t = \rho_0 + at \qquad (4)$$

where ρ_0 and a are constant for a particular metal.

1.5.2.Impurity influence

Impurities in an element act as a scattering center and in turn help to increase the resistivity of the element. As the amount of impurity in metal increases, the resistivity increases [52].

$$\rho_i = Ac_i(1-c_i) \tag{5}$$

where A is composition independent constant, function of both impurity and host metals, c_i is impurity concentration in atom fraction.

For a two phase allow with α and β phase, the resistivity is approximately given by

$$\rho_i = \rho_\alpha V_\alpha + \rho_\beta V_\beta \tag{6}$$

where V is the volume fraction of each phase, ρ is the resistivity of each phase.

1.6. Copper database (microstructure, mechanical and physical properties)

Tables 2, 3, 4, 5 and 6 enlist microstructural, mechanical, thermal, electrical and various other properties related to Cu.

Table 2
Microstructural properties of Cu

Microstructure	
Crystal Structure	Face Centered Cubic
Atomic Radius	1.35 Å
Atomic number	29
Atomic weight	63.546 $g \cdot mol^{-1}$
Electron configuration	$1S^2 2S^2 2P^6 3S^2 3P^6 3D^{10} 4S^1$

Table 3
Mechanical properties of Cu

Mechanical properties	
Modulus of Elasticity	110Gpa
Bulk Modulus	140Gpa
Poisson's Ratio	0.343
Shear Modulus	46Gpa
Hardness, Vickers	369Mpa
Tensile Strength, Yield	33.3Mpa
Elongation at Break	60%

Table 4
Thermal properties of Cu

Thermal properties	
Specific Heat Capacity	0.385 J/g-°C
Thermal Conductivity	385 W/m-K
Melting Point	1083.2 – 1083.6 °C
Thermal Expansion	(25 °C) 16.5 $\mu m \cdot m^{-1} \cdot K^{-1}$

Table 5
Electrical properties of Cu

Electrical properties	
Electrical Resistivity	1.7e-006 ohm-cm

Table 6
Miscellaneous properties of Cu

Miscellaneous properties	
Grain Boundary Energy	625mJ/m^2
Stacking Fault Energy	45 mJ/m^2
Twin Boundary Energy	24 mJ/m^2

2. EXPERIMENTAL

2.1. Sputter deposition

Single crystal copper thin films were sputtered on to Silicon substrates of different crystallographic orientations. (Si (100), Si (110), Si (111) and SiO_2). 99.999% pure Cu target was deposited using custom made four ion gun magnetron sputtering device, which was evacuated to a base pressure of 5×10^{-5} Torr before deposition. The substrate were etched in 10 percent HF-deionized water and the substrate were neither heated nor cooled during the deposition, this gave a very clean single crystal silicon substrate free from silicon dioxide layer. The deposition rate was varied from 1.0-2.0nm/sec, the deposition rate was controlled by controlling the dc power supply to the magnetron guns and entire deposition was done at room temperature.

Cylindrical and planar types of magnetron sputtering systems are widely used for thin film depositions. Several hundred Gauss of magnetic field is generated by permanent magnets embedded in the cathode. Sputtering process is widely in use for the deposition of magnetic materials, this is made possible due to improved design or the magnetic flux distribution with a strong permanent magnet (rare-earth metal) [19]. A base pressure around 10^{-5} to 10^{-3} is maintained and the deposition rate R is given by

$$R = \frac{kW_0}{t} \tag{7}$$

where $k= r_c/r_a$ for cylindrical system, r_c is cathode radius, r_a is anode radius, t is the sputtering time, W_0 is the amount of sputtered particles from the unit cathode area

$$W_0 = \left(\frac{j_+}{e}\right) St \left(\frac{A}{N}\right) \tag{8}$$

where, J_+ is the ion current density at cathode, e is the electron charge, S is the sputter yield, A is the atomic weight of sputtered material, N is the Avogadro's number, t is the sputter time

2.2 X-ray diffraction

X-rays can be defined as "electromagnetic radiations in the wavelength regions around 1A" [56]. X-ray tube usually operates by the acceleration of electrons to high energy and allowing then to strike a metallic target. Using X-rays one can investigate the structure of matter at the molecular level and is commonly engaged for the determination of positions of atoms in a crystalline structure. It is an analytical technique, where a single crystal is bombarded with X-rays to produce a diffraction pattern which in turn are recorded and analyzed systematically to study the nature of the crystal. Bruker D8 Discover equipment was used for this study.

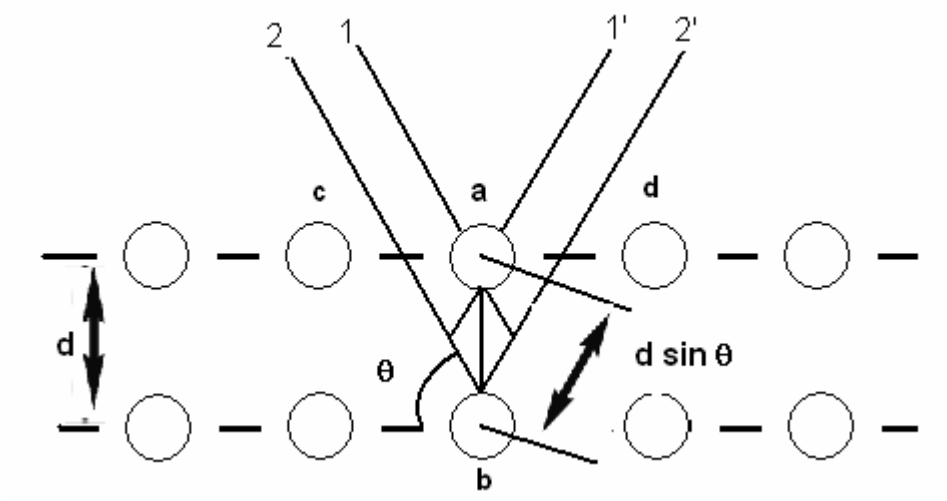

Figure 12 Parallel rays reflected from points with partial reflectivity obeying Bragg's law

In order for the diffraction to occur, the obstacles should be regularly spaces; they should be capable of scattering the wave and have spacing that comparable in magnitude to the wavelength. Now when an X-ray impinges on to a solid material, there is some portion of the beam that is scattered by the electrons of the atoms, now if the beam was incident at an angel theta the constructive interference of the scattered ray will also occur at the same angle with the plane. Now the length traveled by the beam 2-b-2' is more than the length traveled by 1-a-1' by cb + bd and is equal to the whole number 'n' of wavelengths as seen in figure 12.

$N\lambda = cb + bd$

$n\lambda = d_{hlk}\sin\theta + d_{hlk}\sin\theta$

$n\lambda = 2d_{hlk}\sin\theta$ (9)

where d_{hlk} is the *d* spacing between the two atomic plane.

This is known as the Bragg's law [57].

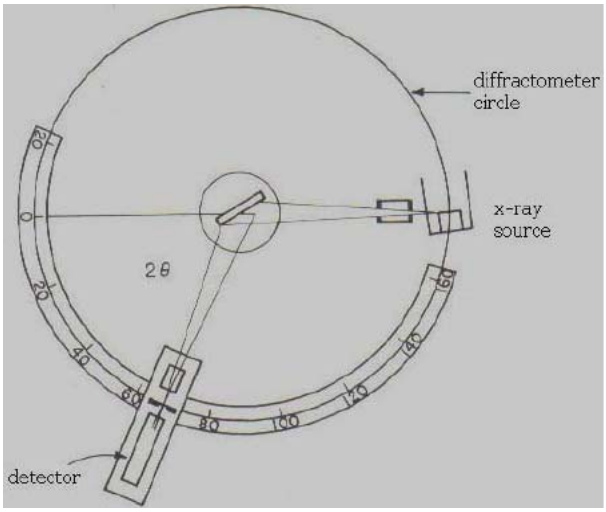

Figure 13 Schematic representation of a diffractometer [22]

A diffractometer is a common apparatus used to determine the angle at which diffraction occurs (See figure 13), specimen is in the form of plate is supported in order to incorporate the rotation about its axis (perpendicular to the page). Diffractometer generates a monochromatic X-ray beam whose intensities are recorded. The counter and the source are on the same plane and can rotate. The carriage and the specimen are couples so the rotation of the specimen by and angle theta will accompany rotation of angle 2 theta by the counter. As the counter moves at constant angular velocity the recorder records beam intensities of the beam diffracted [22].

2.3. Transmission electron microscopy

TEM is playing an important role in materials research; more recently thin film science has found the use of TEM in variety of configurations [58-60]. A perfectly normal eye can resolve points that at about 0.1-0.2mm apart and any instrument that can reveal details finer that 0.1mm can be called as a microscope [61]; any microscope using electrons to do this is basically an electron microscope. Like many other types of electron microscope TEM is also composed of a number of different systems, working in tandem to form a unit capable of imaging thin specimens. Electron guns and condenser lenses give rise of radiation striking thin specimens form the illumination system, where as specimen manipulation and imaging systems are composed of specimen stage, holders, and objective, intermediate and projector lenses [62].

Transmission electron microscopy was done in order to look at plan view and cross-sectional sample of 1.5μm thick copper thin film on different silicon substrates. The bright-field and diffraction pattern images were taken using a JEOL JSM 2010 electron microscope, with a lanthanum hexaboride (laB_6) filament gun, acceleration voltage used during the process was 200KV. The JEOL JSM 2010 Transmission electron microscope has a resolution of 0.23nm and a tilt limit of +/-30 degrees; the images taken by the camera are developed in the form of negatives. The negative are then scanned using Epson 4870 scanner and are then processed with the help of Adobe Photoshop CS2 software.

2.3.1 Sample preparation technique for TEM

One of the major limitations of the TEM is its sample preparation; the specimens for TEM should be thin or in other words should be electron transparent. Today TEM sample preparation methods exist for almost all the material known. The methods used for the sample preparation for this study are as follows:

2.3.1.1 Plan-view sample preparation

A slice (about 2 × 2mm) of copper over silicon was cut with the help of diamond tip cutting pen. The slice is then cleaned gently using acetone so as to remove all the impurities on the surface of the copper film; slice is bonded to polishing crystal cylinder with copper film facing down, so that the silicon substrate could be polished. The slice was polished to an approximate thickness of 100μm using allied tech MetPrep polisher, followed by dimpling by 3μm copper wheel and 1μm polishing cloth to a final thickness of about 10-15μm on Gatan dimple polishing machine. The specimen was then ion milled to obtained the required electron transparency by using Gatan Precision Ion Polishing System, with ion beam energy at 4KeV, double beam configuration, both top guns at angle 5.5° and sample rotation at 3rpm. Schematic representation of the process is shown in figure 14.

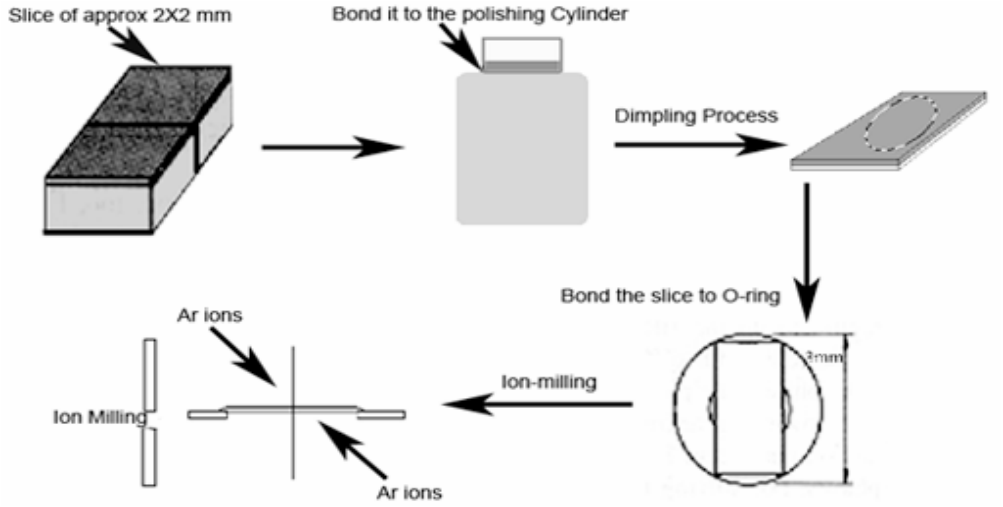

Figure 14 Systematic representation of plan-view sample preparation

2.3.1.2 Cross-section sample preparation technique

Two nearly equal slices of copper thin film on silicon were cut with the help of diamond pen. This was done my scratching away silicon on the silicon substrate, so that they form a site for cracks to propagate and then the silicon is tapped lightly till the slice breaks. The two slices were then cleaned in alcohol and were bonded together face to face with the help of resin bond. As the single crystal copper samples cannot be heated they were placed in spring loaded die for 5 days, to let the bond set.

The samples were then removed gently from the die and bonded on to a polishing crystal cylinder with the help of crystal bond. Then the samples were put through a series of mechanically grinding and polishing processes to get final surface with 1μm surface roughness. Once smooth surface was obtained the sample was removed and

polished on the opposite side to a total thickness of 100μm.The sample was then dimpled on Gatan dimple polishing machine. After dimpling process a molybdenum O-ring was bonded (resin bond) to the sample, to support it. Sample was then ion milled in Gatan Precision Ion Polishing System, with ion beam energy at 4KeV and sample rotation at 3rpm. Schematic representation can be viewed in figure 15.

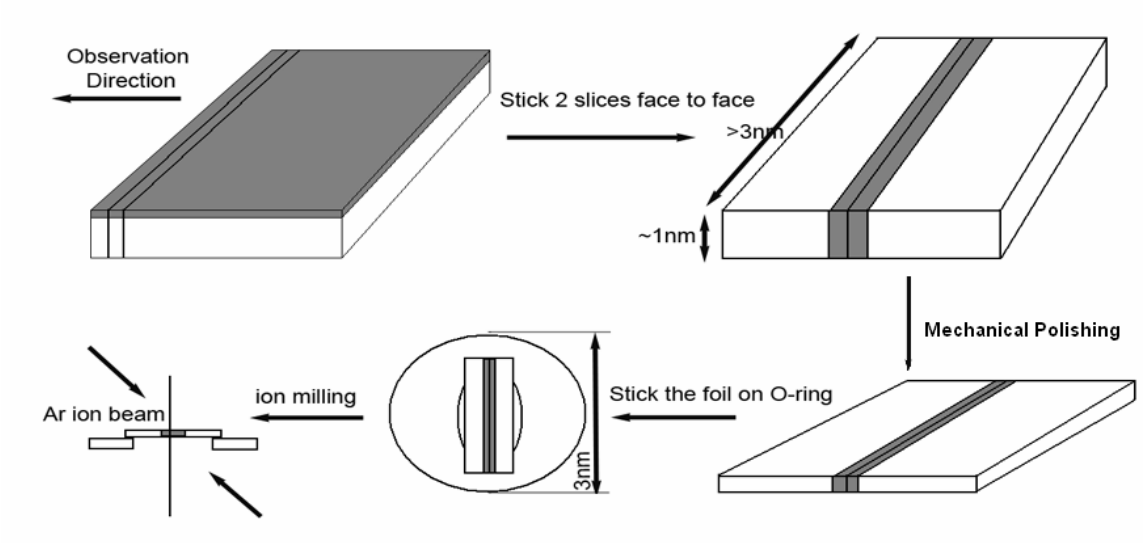

Figure 15 Systematic representation of cross-section sample preparation

2.4. Nano-indentation hardness measurements

Indentation has been a common technique for the hardness measurement from many years and involves a fixed load applied to an indenter, and the resultant indentation is observed in figure 16. Hardness is the load on the indenter divided by the projected area of the indentation [63]. There is no physical property measured in this test, but hardness of a material is directly affected by the yield strength or the stiffness of the material.

In a thin film material, indentation in the range of micrometers may go through the thickness of the material onto the substrate and so the measured hardness would a convoluted value of film and substrate. So, an indentation in the range of nanometers is required. These instruments measure both load on the indenter and its displacements during the course of indentation, hence are called depth-sensing indentation [64-68].

Hardness measurements for this study were conducted on Ficherscope HM2000Xyp hardness tester, for every sample, hardness was measured at an indentation depth of 100nm to 250 nm with an interval of 25 nm and for each indentation depth an array of 9 indentations were preformed i.e. for each sample a total of 63 indentations were performed. Indentation load was set to be 300mN and a complete indentation cycle was completed in 30secs.

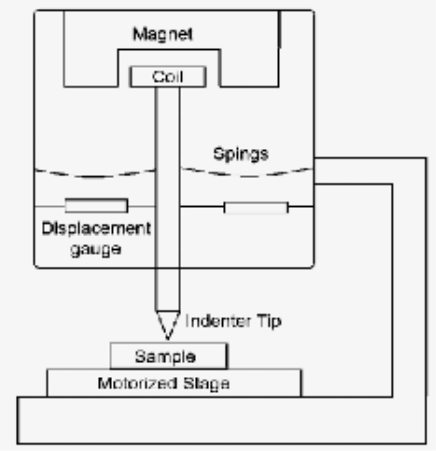

Figure 16 Block diagram of nanoindenter [51]

2.4.1 Determination of indentation hardness

In order to calculate indentation hardness, it is assumed that all the deformations during unloading of indenter are elastic. Following are the sequential description of indentation process (See figures 16, 17 and 18):

- Indenter is presses against the sample with load ‘P’
- Displacements are caused by both elastic and plastic deformation of the specimen
- Indenter is retreated
- All the elastic deformations are recovered
- Residual indentation may remain

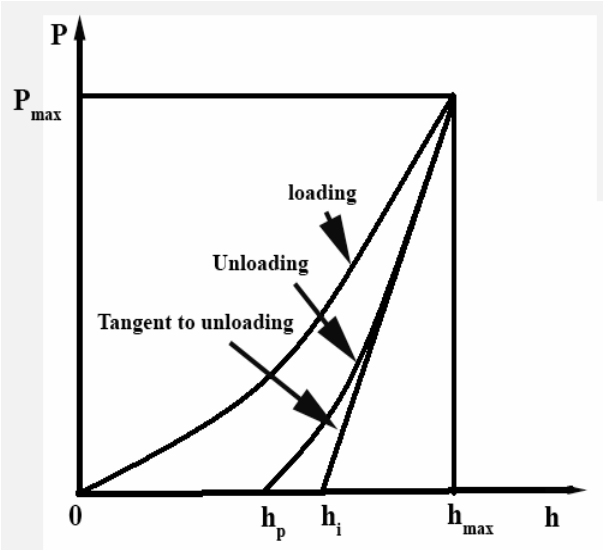

Figure 17 Schematic representation of an indentation hardness curve [51]

Indentation hardness is defined as the ratio between maximum load and the projected area between the indenter and specimen i.e.

$$H_{IT} = P_{max} / A_c \quad (9)$$

where $A_c = f(h_c)$ (10)

h_c is the height of contact of indenter with the specimen and is given by,

$$h_c = h_{max} - \varepsilon (h_{max} - h_i) \quad (11)$$

ε is a function of shape of indentation tip and its values are presented in table 7.

Table 7
A systematic representation of various indenter geometry and corresponding ε values

Indenter shape	**ε**
Flat punch	1.0000
Cone	0.7268
Sphere	0.7500
Paraboloid	0.7500

The value of *f* in equation 2 is defined of every type of inventor in International Standards. For Vickers indenter the value of '*f*' is 24.50

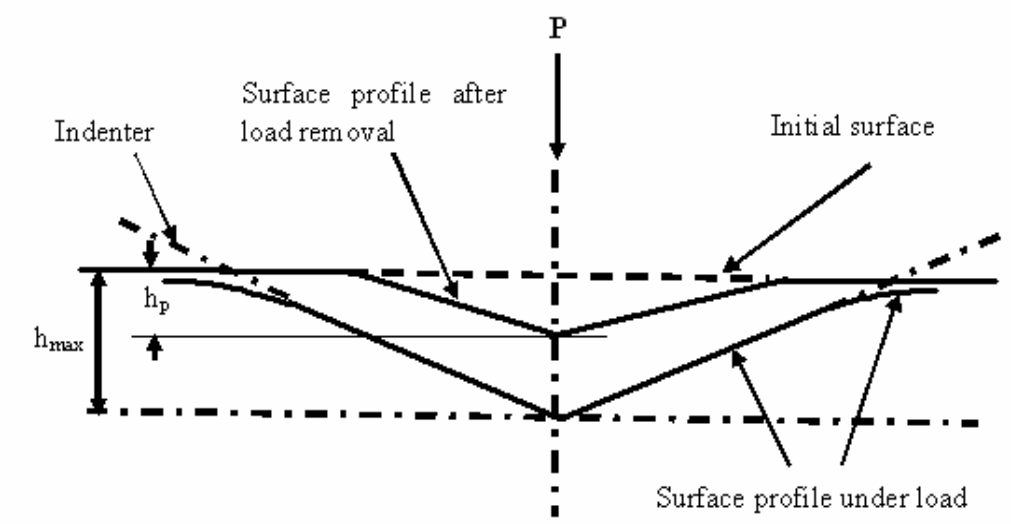

Figure 18 Schematic diagram of an indenter with various terminologies used in calculations

2.4.2 Determination of indentation modulus

For indentation modulus measurement it is assumed that the 'compliance of the sample and of the indenter tip can be combined as springs in series' [69].

$$\frac{1}{E_r} = \left(\frac{1 - v_{indentor}}{E_{indenter}}\right) + \left(\frac{1 - v_{IT}}{E_{IT}}\right) \tag{12}$$

where E_r is the reduced modulus, $E_{indenter}$ is the indenter modulus, E_{IT} is the indentation modulus, $\upsilon_{indenter}$ is the Poisson's ratio for the indenter, υ_{IT} is the Poisson's ratio for the specimen.

Contact stiffness is defined as the slope of the Force/Loading curve during unloading cycle (See figure17) [70]

$$S = \frac{dP}{dh} = \frac{2 E_r \sqrt{A}}{\sqrt{\pi}} \tag{13}$$

where A is contact area.

Value of reduced modulus can be obtained from equation (2) and can be substituted in equation (1) to get the value of indentation modulus, i.e.

$$E_{IT} = (1 - v_{IT}^{\,2}) \Big/ \left\{ \frac{2}{\sqrt{\pi}} X \frac{\sqrt{A(h_c)}}{S} - \frac{(1 - v^2_{indenter})}{E_{indenter}} \right\} \tag{14}$$

2.5. Four point resistance test

Four point probe resistant test setting was used for the resistivity measurements, from 0 K to 300 K. Four point probe resistance measurement test is relatively a very simple resistance measurement technique, without any curve fitting process and any need to the measurement of physical dimensions of the resistor. A common four point probe consists of diffused semiconductor resistor R extending between contacts *a* and *b*. There are two more contact *c* and *d* for the purpose of contact making (See figure 19).

A precaliberated current is sent from the point *a* to point *b* and resultant voltage drop between *c* and *d* is measured. The resistance between *c* and *d* can be calculated by known current and the measured voltage. Current is then passed between *c* and *d* and the resulting voltage loss is measured. The resistance of resistor *R* between points *c* and *d* and value of the contact resistance at contact *a* and *b* are calculated using the known current and the measured voltage. From these measurements the value of contact resistance can be easily extracted using Ohm's Law. [71].

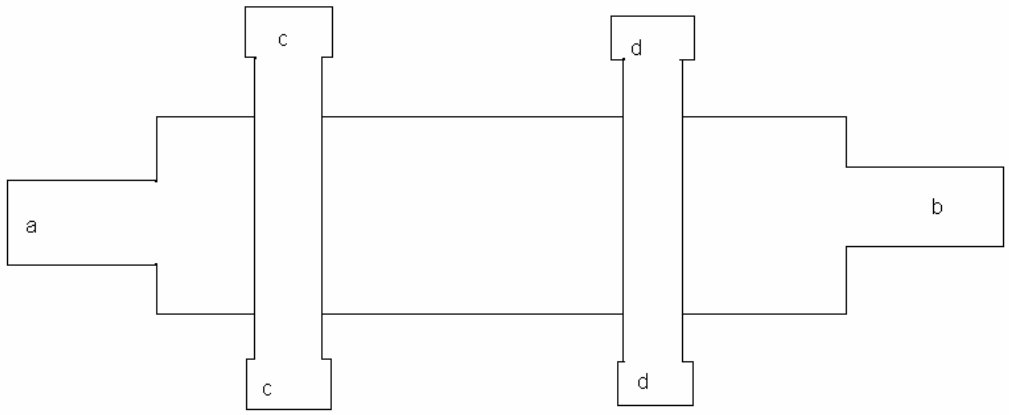

Figure 19 A schematic representation of four point probe

3. RESULTS

3.1 Microstructure

3.1.1 X-ray diffraction

Copper was sputter deposited onto Si(100), Si(110) and SiO_2 using magnetron sputtering technique at deposition powers of 100W, 200W, 600W and 800W. X-ray diffraction was done on all the samples to examine microstructures. X-ray diffraction patterns are shown in Figure 20 for Cu films grown on Si (100) substrates, only very strong copper (200) peaks can be seen all specimens together with Si (400) peak.

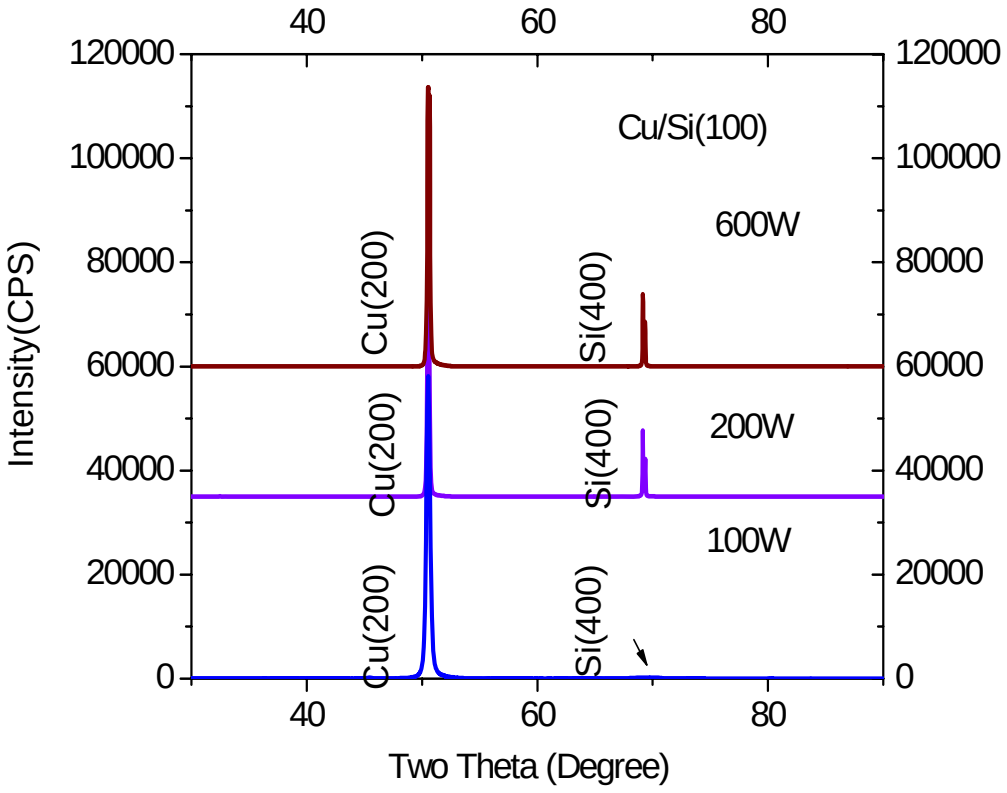

Figure 20 X-Ray results of Cu film deposited on Si (100) substrate at 100W, 200W, 600W deposition power

X-ray diffraction patterns of copper films on silicon (110) substrates revealed only strong Cu (111) peaks at 43.3 degrees and strong Si (220) peaks at 47.5 degrees, as seen in figure 21. X-ray diffraction studies were conducted for Cu films deposited at all deposition powers, and similar results were observed in all other cases.

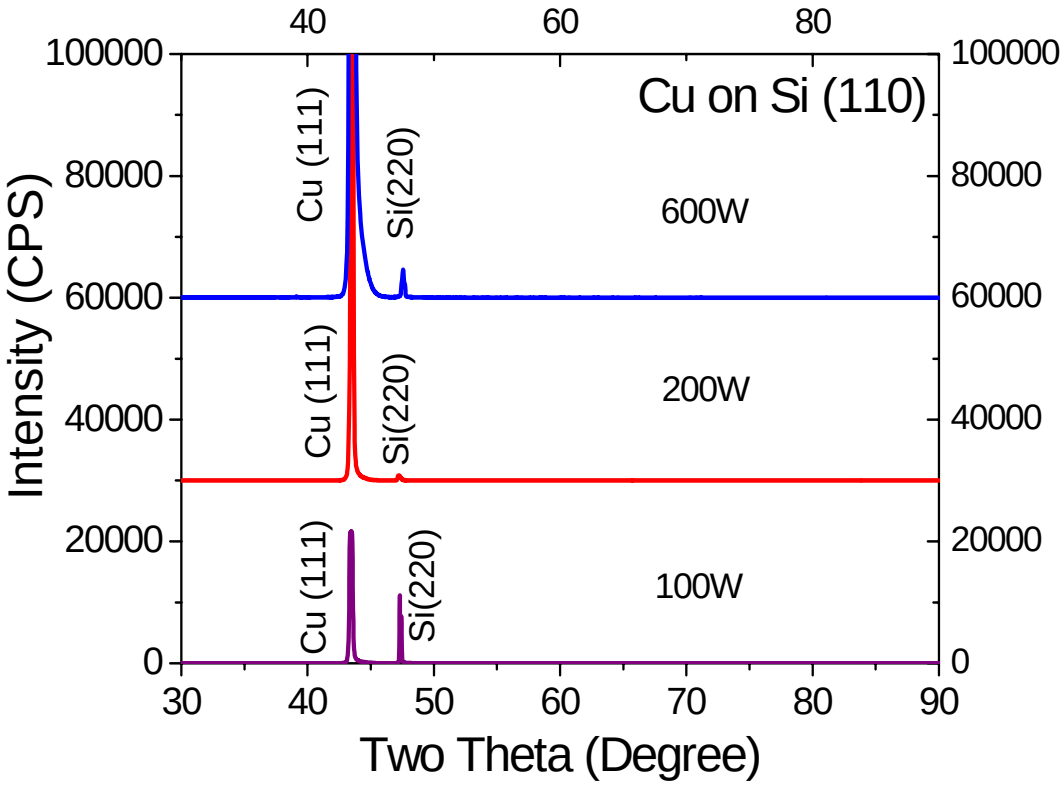

Figure 21 X-Ray results of Cu film deposited on Si (110) substrate at 100W, 200W, 600W deposition power

X-ray diffraction results for copper on silicon dioxide showed strong Cu (111) peak as well as much weaker Cu (200) diffraction peaks, very typical for polycrystalline Cu films grown on silicon dioxide (See figure 22).

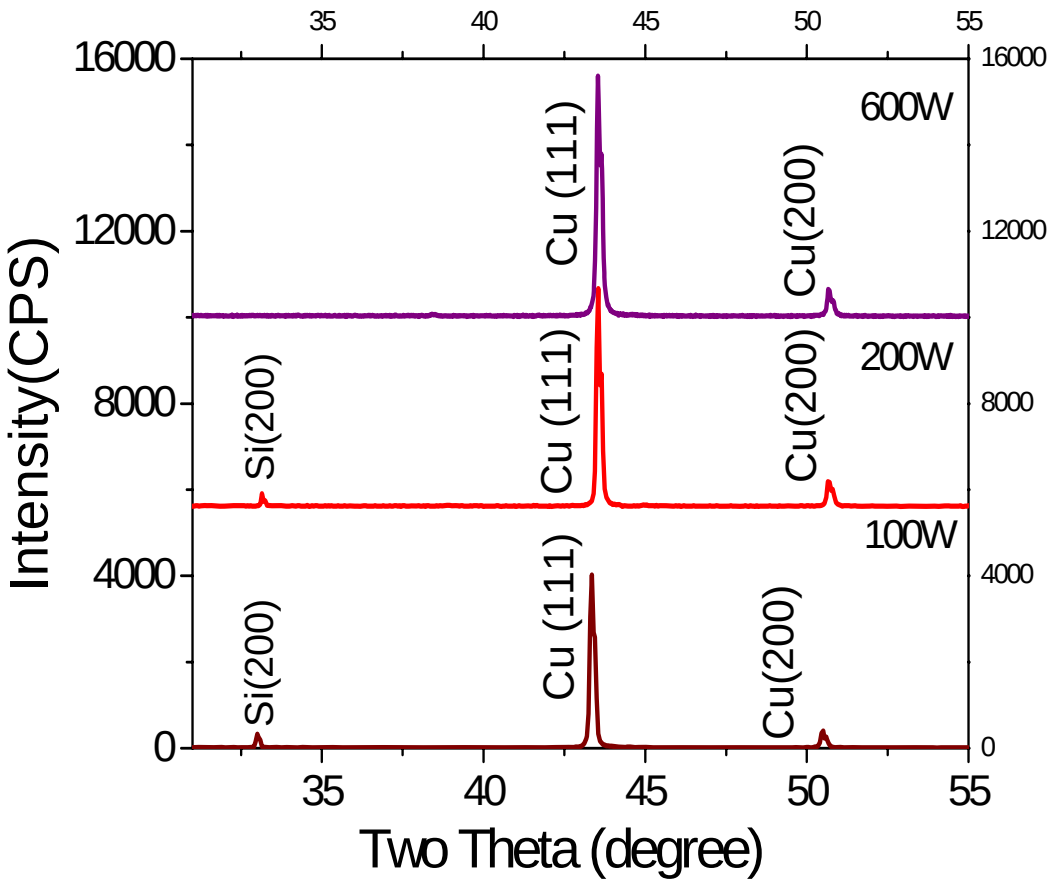

Figure 22 X-Ray results of Cu film deposited on SiO_2 substrate at 100W, 200W, 600W deposition power

3.1.2 Transmission electron microscopy

To further study microstructural details, JEOL 2010 was used for transmission electron microscopy analysis. Sample preparation for plan-view and cross-section samples are presented in detail in experimentation section.

3.1.2.1 Cu films on Si (100)

Figure 23 is the cross-sectional transmission electron microscopy (XTEM) image of Cu on Si (100). Grain boundaries are not detected. The diffraction patter clearly shows the arrangement on single crystal copper (100) grown on silicon (100) substrate.

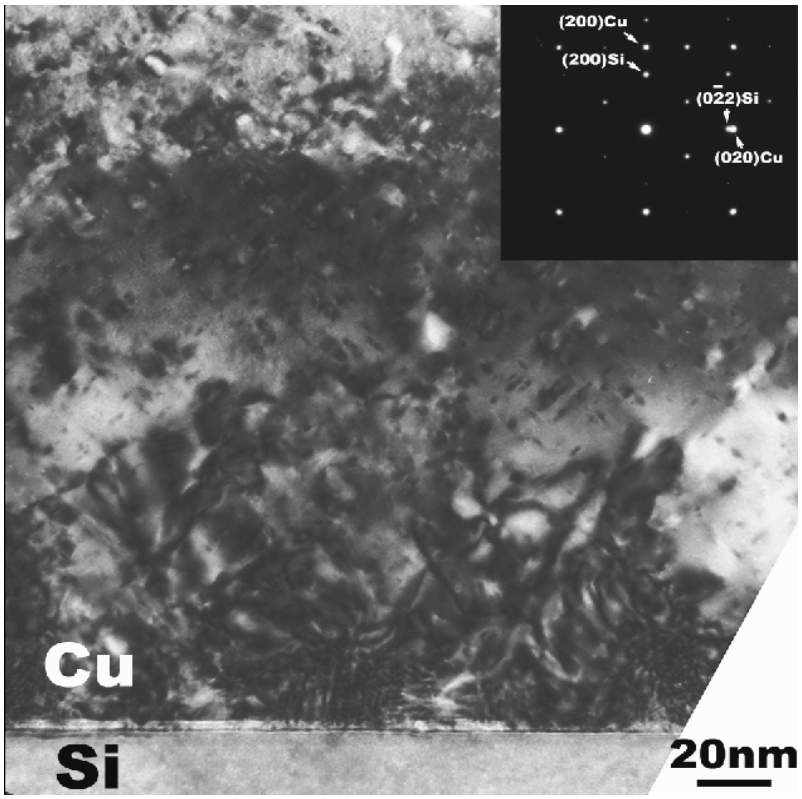

Figure 23 XTEM image of Cu films grown on Si(100) shows no grain boundaries. Contrast is mostly originated from dislocations. Diffraction pattern indicates that Cu (100) single crystal films were grown on Si (110) substrate.

At lower magnifications, the cross-sectional TEM micrograph of Cu films alone, as shown in Figure 24, clearly shows a network of dislocations in copper without any sign of grain boundaries.

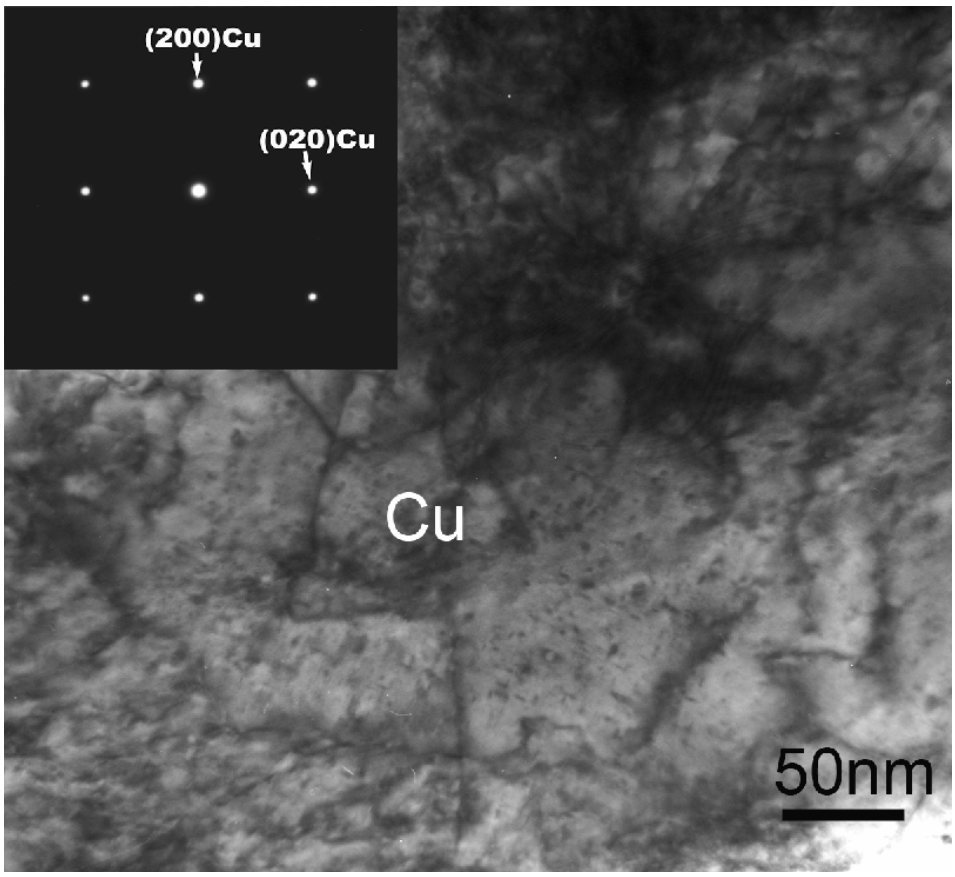

Figure 24 XTEM image of Cu films grown on Si(100) shows no grain boundaries. A network of dislocations is seen. Diffraction pattern indicates that Cu (100) single crystal films were grown on Si (110) substrate

3.1.2.2 Cu films on Si (110) substrate

TEM studies of Cu films grown on silicon (110) were performed to examine the microstructure of Cu films from two different orientations: namely Si [111] and Si [112]. Si (110) is a special substrate, where two different orientations may be obtained during sample preparation. As shown schematically in Figure 25, these two orientations are Si [111] and Si [112] and are perpendicular to each other. Figure 26 shows Cu film on Si (110) substrate from Si (111) zone. Si substrate clearly shows [111] diffraction zone. The copper film shows highly twinned structure, with twin interfaces oriented predominantly parallel to substrate surface. Again no grain boundaries were detected. The diffraction pattern of Cu shows single crystal Cu (111) with twins along Cu (110) diffraction zone. Presence of some kind of impurity can also be detected form the diffraction pattern which comes from TEM sample preparation process.

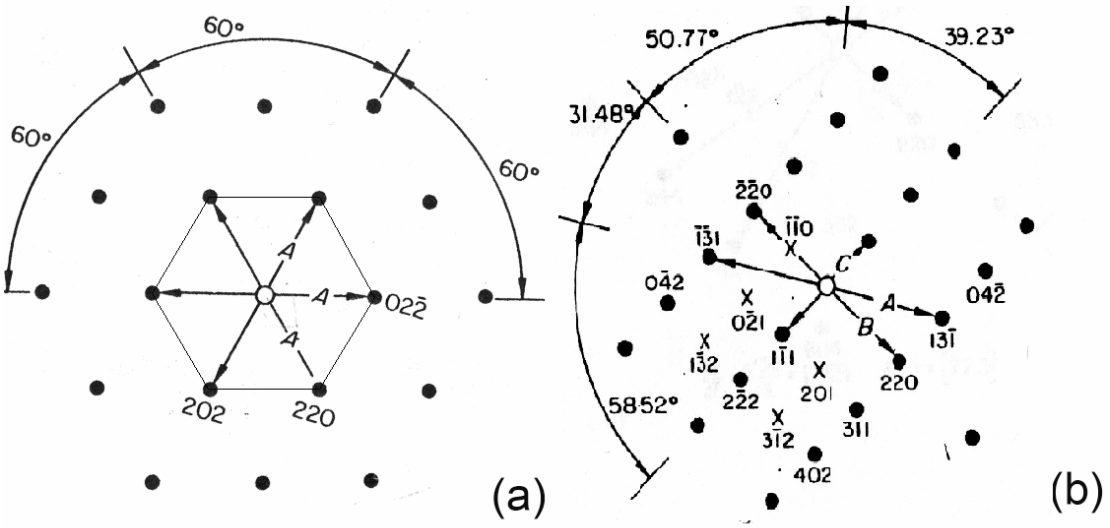

Figure 25(a) The diffraction pattern in Si (111) zone. (b) The diffraction pattern in Si (112) zone.

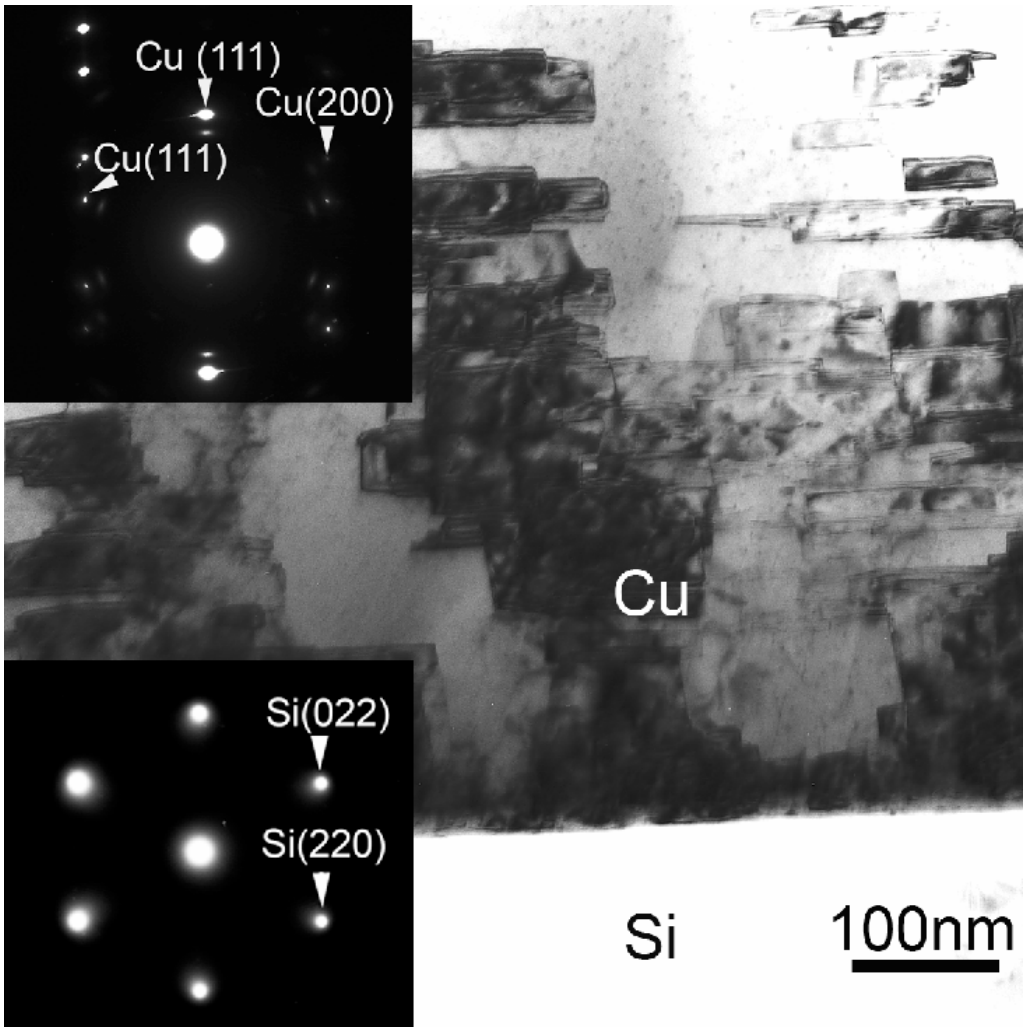

Figure 26. XTEM image of Cu films on Si (110) substrate along Si (111) diffraction zone. Cu films has single crystalline nature with Cu (111) planes and (111) type twin interface parallel to substrate surfaces. The diffraction zone of Cu film is Cu [110].

In Figure 27 (a) we can see another XTEM example of Cu films grown on Si (110) substrate. A very high density of grow twins are clearly seen in the specimen. Again single crystal Cu films were grown with Cu (111) planes parallel to substrate surfaces. Diffraction pattern of Cu confirms that the Cu films indeed has single crystalline nature with (111) type twin interface orientated parallel to substrate surface. In twinned Cu films, the Cu [110] zone axis has rotated with respect to each other about one set of common (111) twin plane as shown in Figure 27 (b).

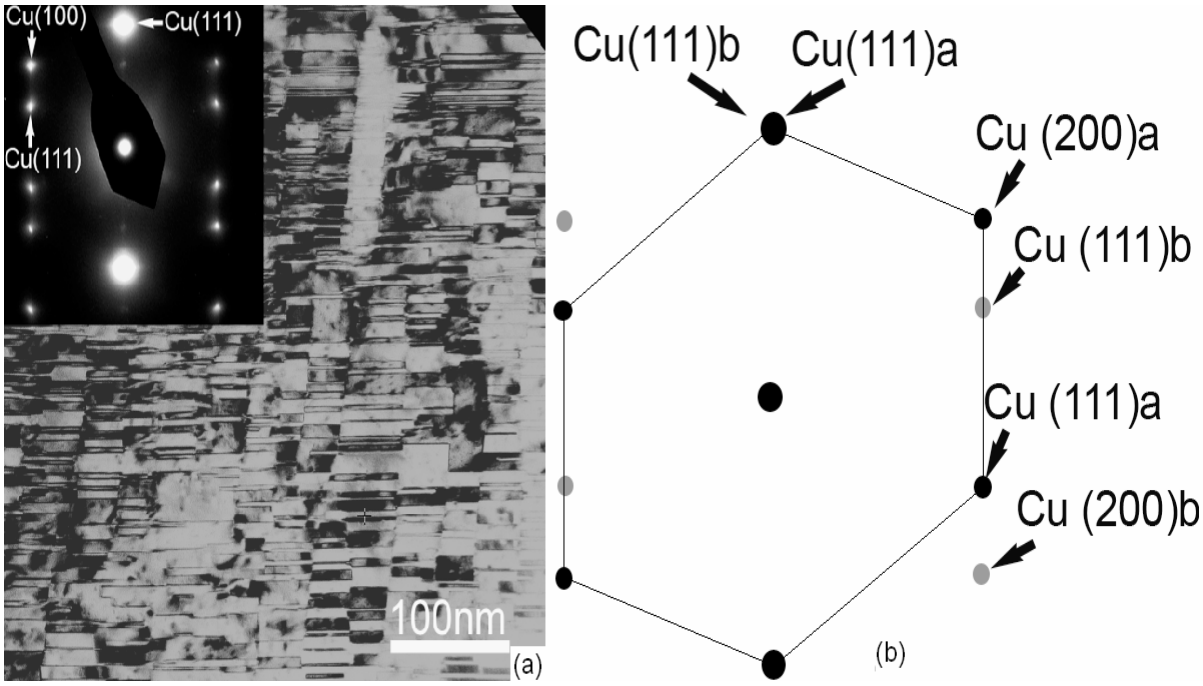

Figure 27 (a) XTEM image of Cu films on Si (110) substrate along Si (111) diffraction zone, the diffraction zone of Cu film is Cu [110].(b) Schematic analysis of the diffraction pattern, indicating the twin structure.

Figure 28 shows the same Cu film examined along Si [112] diffraction zone. The high density growth twins seen along Si [110] zone in Figures 27(a) and 26 are not visible in this case. Instead the micrograph shows a large number of dislocations (most of them seems to be threading dislocations) without signs of grain boundaries. The diffraction patter shows single crystal Cu films with Cu [112] diffraction zone parallel to Si [112] diffraction zone with however 90 degree rotation. Cu (111) planes are parallel to substrate surface.

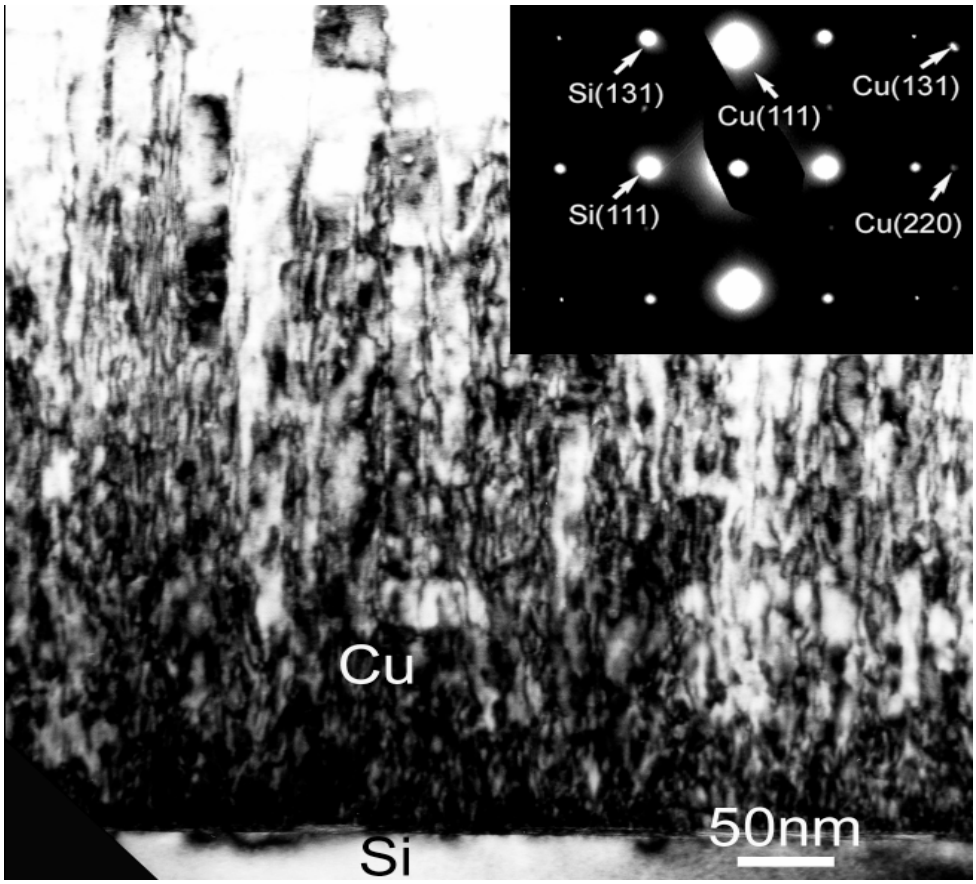

Figure 28 XTEM image of Cu films on Si (110) substrate along Si (112) diffraction zone, the diffraction zone of Cu film is Cu [112]. None of the twinning observed in Cu (110) zone are visible here

3.1.2.3 Cu on SiO_2

It was clearly seen in XRD that Cu films on SiO_2 has polycrystalline nature with strong (111) texture. Plan-view micrograph confirmed Cu films indeed have conventional polycrystalline structure (figure 29). The average grains size measured over number of samples is approximately 400nm. Presence of a large number of twins can also be seen inside Cu grains. Diffraction pattern has shown some impurities originated from TEM sample preparation besides Cu (111) and Cu (200) diffraction rings.

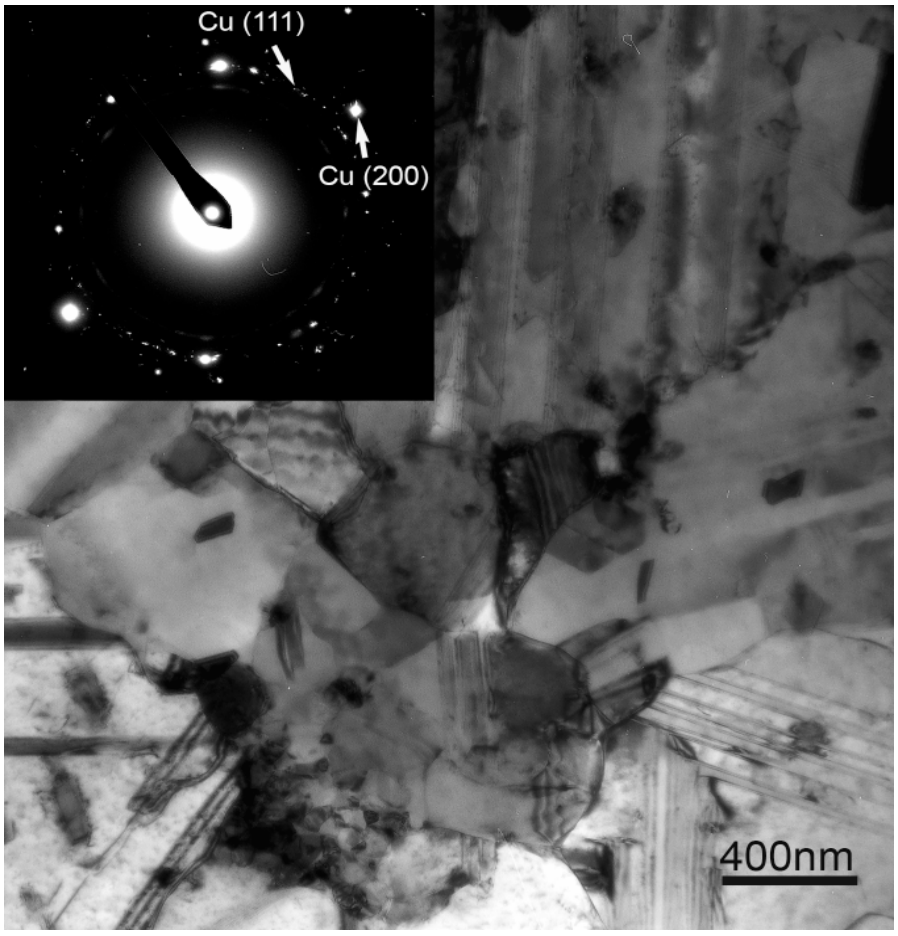

Figure 29 Plan view transmission electron microscope image of Cu on SiO_2 shows grains of about 400nm and highly twinned structure

3.2. Mechanical properties

Conventional uniaxial tensile test are not feasible for thin film due to the dimensional constrains. Instead hardness and elastic modulus of films were measured in all specimens using a Ficherscope HM2000Xyp instrument. The instrument allows accurate measurement of film hardness and indentation modulus as a function of indentation depth using analysis method similar to nanoindentation techniques. In-depth information regarding the data analysis and standard practice of calculations is discussed in experimental section. Figure 30 shows load vs. displacement curve obtained by indentation test on Cu (100) films grown on Si (100) substrate. Maximum load imposed is 250 mN and maximum displacement obtained is 250nm, similar types of tests were done for all other samples. Indentation hardness vs. indentation depths and indentation modulus vs. indentation depths plots are shown in figures 31 and 32, respectively.

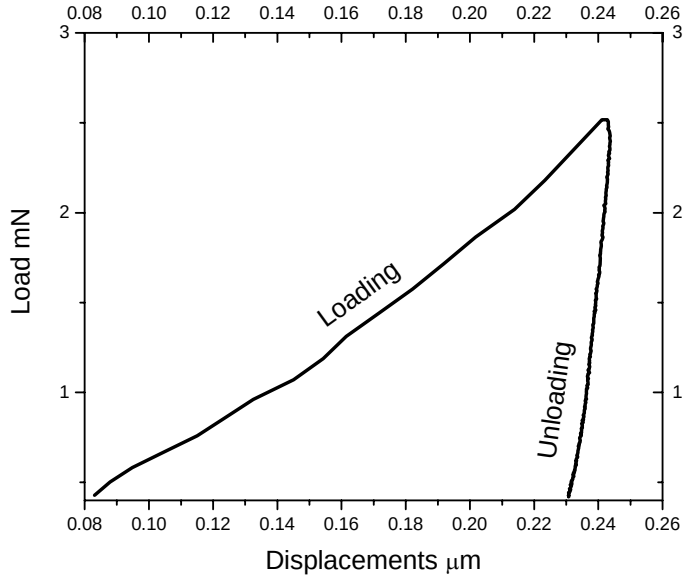

Figure 30. Load vs. indentation depths curve

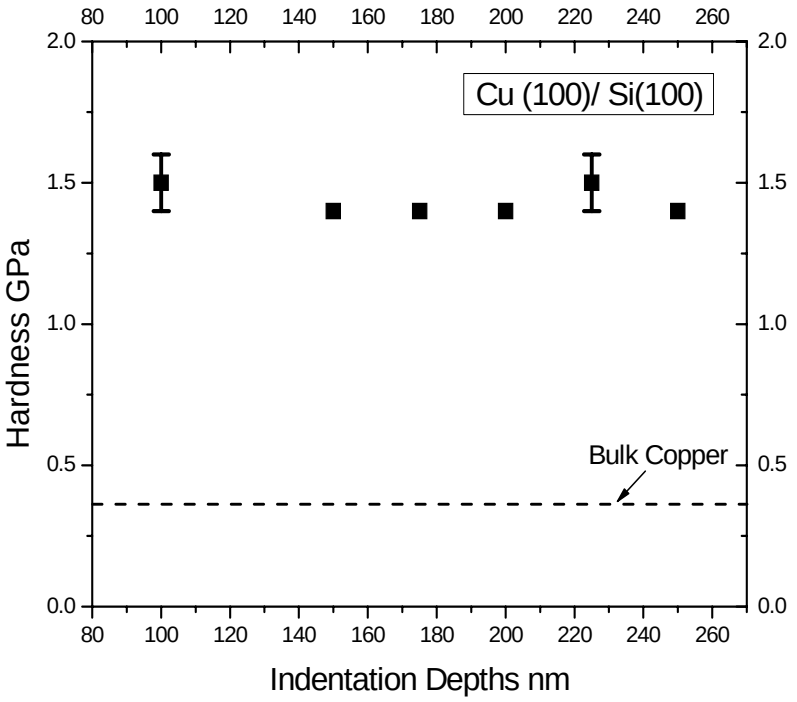

Figure 31. Indentation hardness vs. indentation depths for Cu (100) on Si (100)

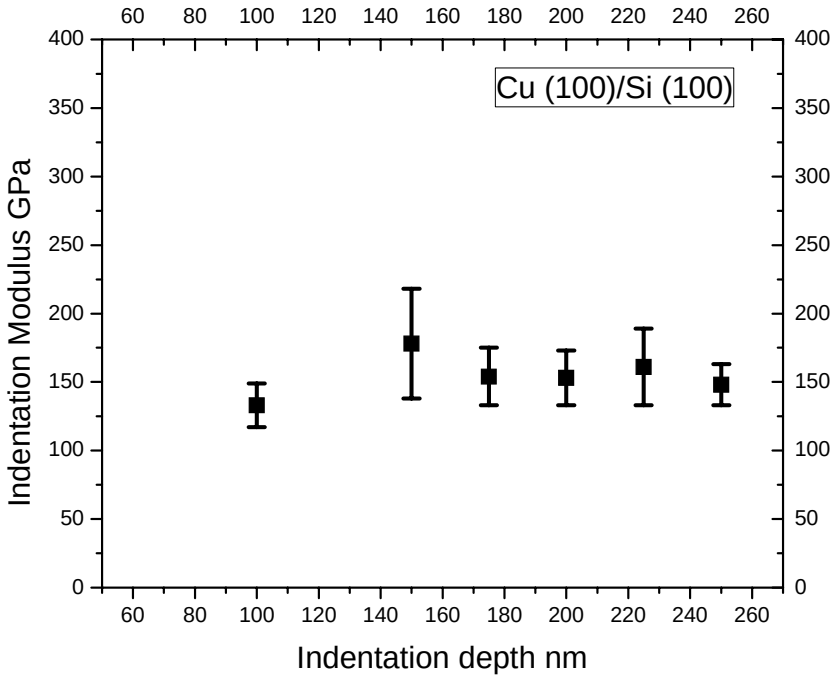

Figure 32. Indentation modulus vs. indentation depths for Cu (100) on Si (100)

3.2.1 Indentation hardness

Figure 31 shows indentation hardness vs. indentation depth plot for Cu (100) films grown on Si (100) substrate. Single crystal Cu (100) deposited on Si (100) shows and average indentation hardness of 1.4 Gpa (figure 33). Highly twinned single crystal Cu (111) deposited on Si (110) Figure 34 shows an average indentation hardness of 2.2 Gpa, 6 times greater than that of the conventional bulk Cu. ~ 0.36Gpa. Copper films deposited on SiO_2 have an average indentation hardness of 2.5 Gpa, Figure 35. Hardness results are reproducible by comparing different sets of data.

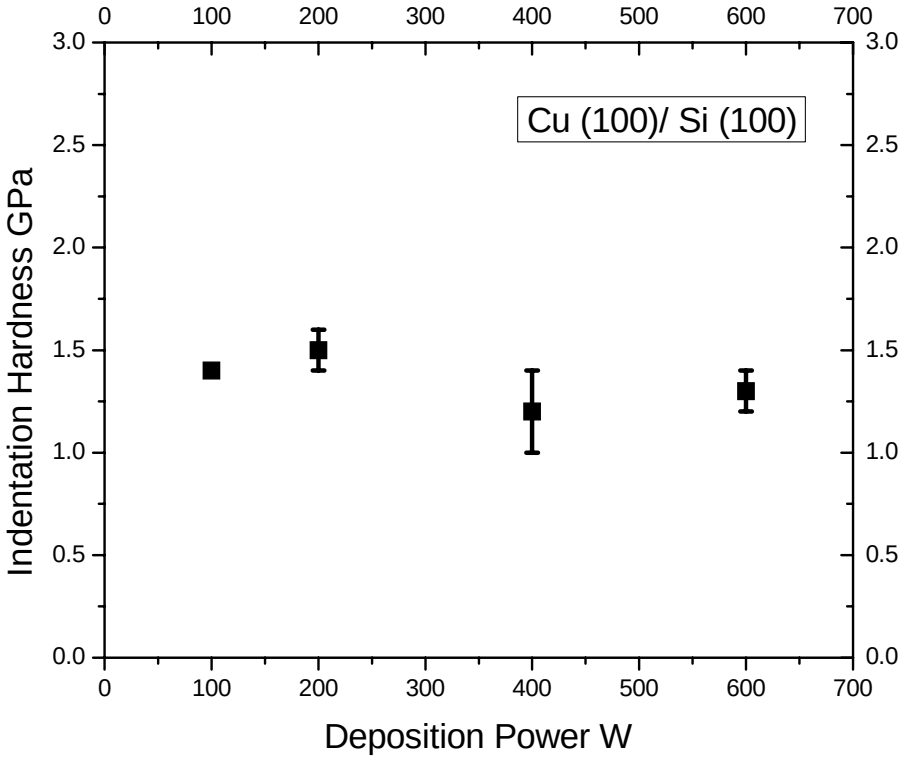

Figure 33 Indentation hardness vs. deposition power plot for Cu (100) on Si (100)

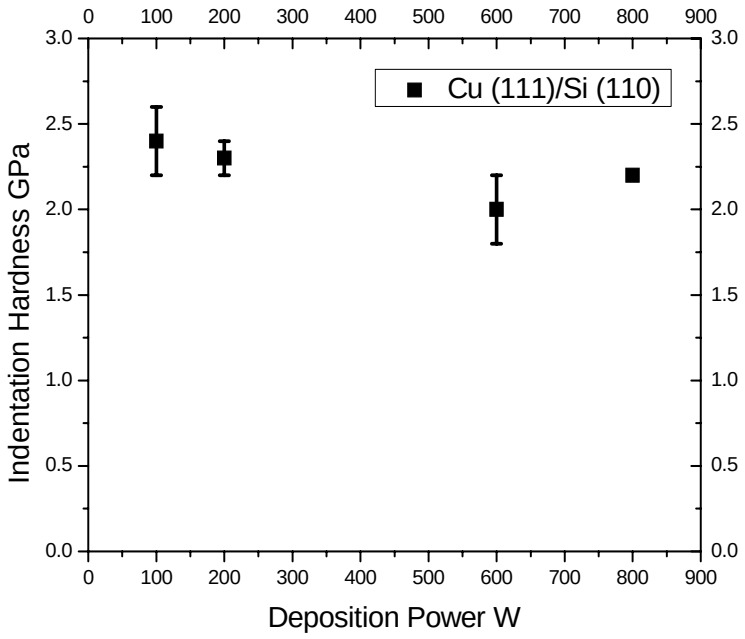

Figure 34 Indentation hardness vs. deposition power plot for Cu (111)/Si(110)

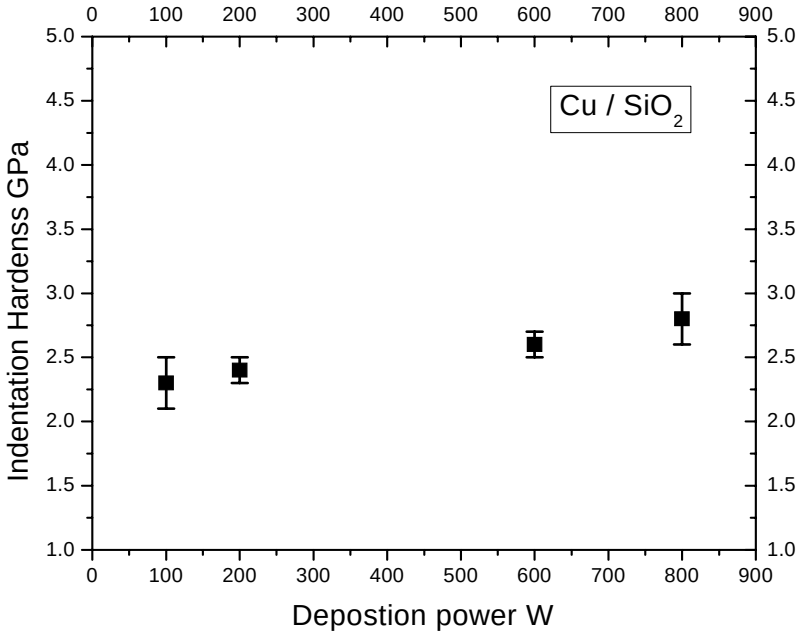

Figure 35 Indentation hardness vs. deposition power plot for Cu on SiO_2

3.2.2 Indentation modulus

Indentation modulus for as-deposited Cu was calculated from the results of nanoindenation tests. Figure 32 shows hardness vs. indentation modulus plot for Cu (100) on Si (100) similar plots were plotted at every deposition powers and averaged over. The procedure for these calculations is clearly mentioned in experimental section. Single crystal Cu (100) on Si (100) reported an average indentation modulus of 133 Gpa, comparable to that of bulk Cu, ~ 120 Gpa. Single crystal Cu (111) on Si (110) reported an average indentation modulus of 134Gpa and Copper on SiO_2 has an average indentation modulus of 125 Gpa (See figures 36, 37 & 38).

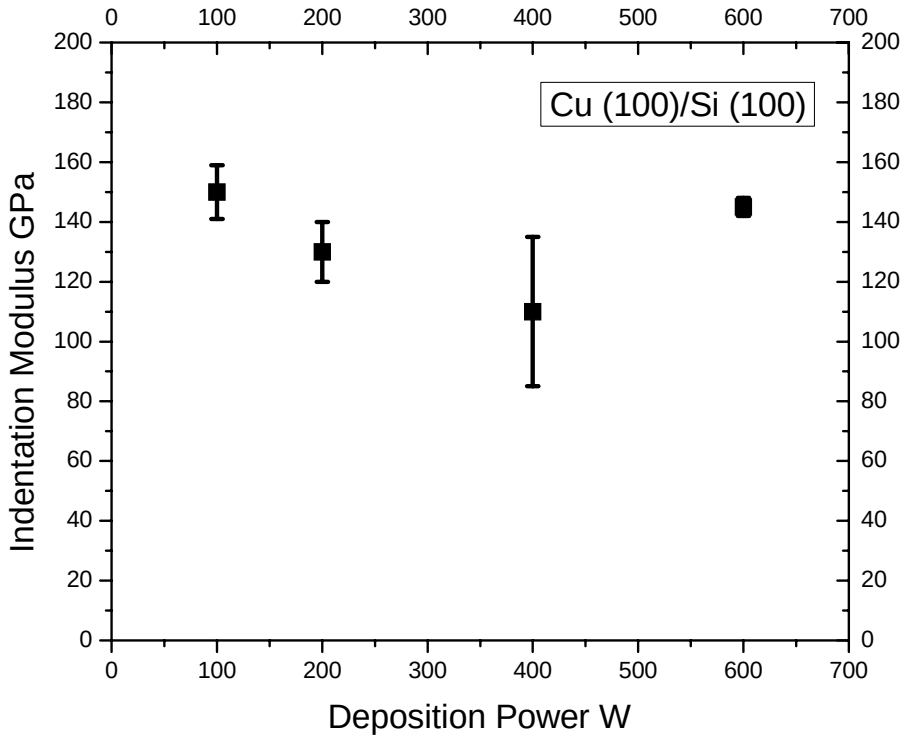

Figure 36 Indentation modulus vs. deposition power plot for Cu (100) on Si (100)

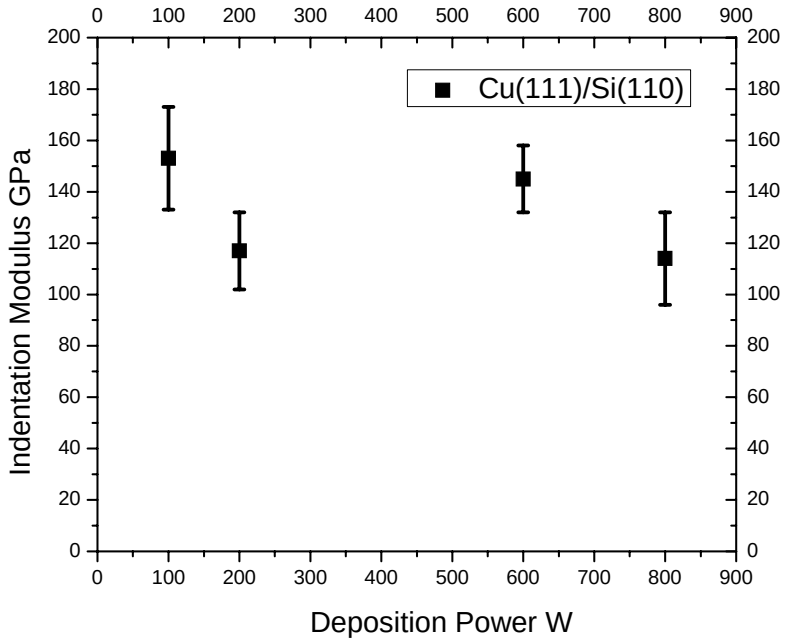

Figure 37 Indentation modulus vs. deposition power plot for Cu (111) on Si (110)

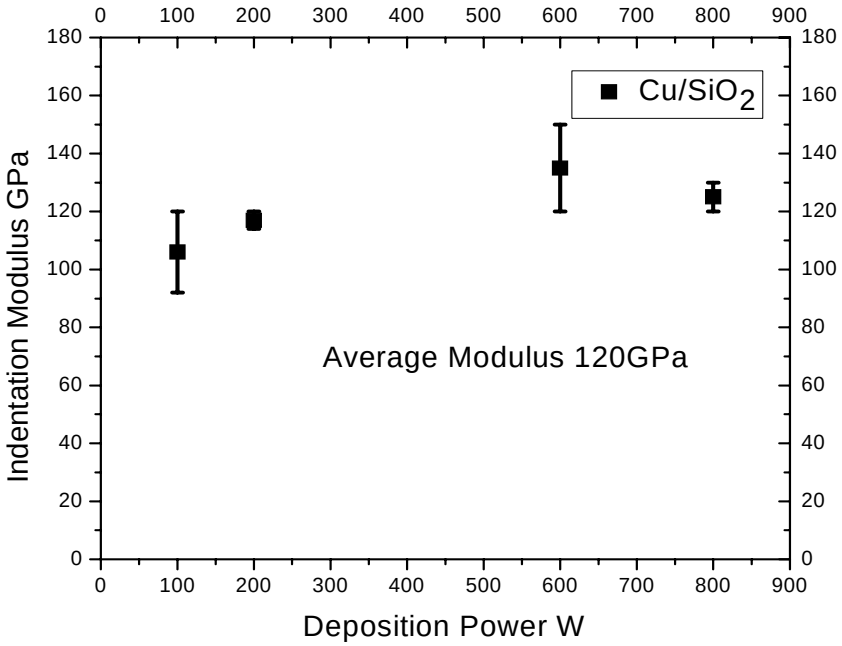

Figure 38 Indentation modulus vs. deposition power plot for Cu/SiO_2

3.3. Electrical properties

Four point resistivity tests were done on as-deposited single crystal Cu (100), Cu (111) and polycrystalline Cu films on SiO_2. All the samples show a linear increase in resistivity as the temperature increases. Electrical resistivity tests were done from 0 K to 300 K. Repeated measurements show reproducible results. At room temperature (298 K) the resistivity measurement for Cu (100) in Si (100) was 1.95 ± 0.02μΩ·cm, 2 ± 0.02 μΩ·cm for Cu (111) on Si (110) and 1.90 ± 0.02 μΩ·cm for polycrystalline Cu films grown on SiO_2. These results are slightly higher than that of bulk high purity Cu, ~ 1.75 μΩ·cm at room temperature (See figure 39).

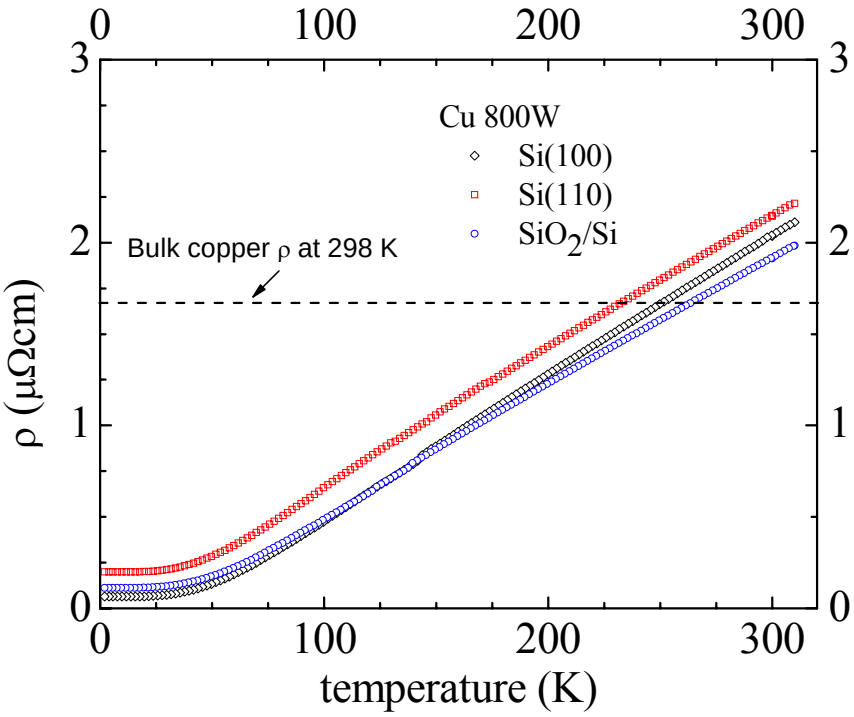

Figure 39 Four point resistivity test results for as deposited coppers on silicon substrates from 0K to 300K

4. DISCUSSION

4.1. Microstructure

4.1.1 Epitaxial growth of copper thin film on Si substrate

There is still no universal theory or law that can predict the epitaxial growth of thin films on substrates, one can predict or understand the epitaxial growth of thin films by geometric matching rule. In a deposition process, maximizing the bond density leads to the minimization of interfacial energy. So is it is favorable for the depositing atom to align themselves with the substrate and grow epitaxially by matching the periodicity and structure of the substrate. In 'homoepitaxy' (thin film material is same as the substrate) the interface energy is zero i.e. the interface disappears into bulk material. In heteroepitaxy this is not possible, but the depositing thin film prefers the orientation with minimum surface energy. Fundamental criterion for epitaxy is fractional mismatch 'f' at the interface. The fractional mismatch in atomic periodicities is defined as [72]:

$$f = 2\frac{(a_f - a_s)}{a_f + a_s} \tag{15}$$

where a_f and a_s are the atomic spacing of thin film and substrate in one direction, f is the fractional mismatch.

If f is smaller than 10% epitaxial growths is said to be possible.

Table 8
Tabulated format of Si and Cu d-spacing

Silicon Orientation hlk	Si'd' Spacing	Copper Orientation hlk	Cu'd' Spacing
111	3.1130	111	2.0871
200	2.6960	200	1.8075
220	1.9063	220	1.2781
311	1.6257	311	1.0899

In the case of Cu films deposited on Si (100), Cu has face center cubic (fcc) structure and Si has diamond cubic structure.The tabulated values of d-spacing for Cu and Si are shown in table 8. The lattice constants are 0.361nm and 0.543nm. If Cu (100) was to grow on Si (100) there is an apparent fractional mismatch of 33 % or 0.33 which is greater than 0.1. But this mismatch (between Cu (100) and Si (100)) decreases to 5% when Cu (100) rotates at an angle of 45 degrees; this can explain the rotation of Cu (100) on Si (100) as seen in the diffraction patterns (figure 40). Diffraction pattern of cross-sectional view of Cu (100) on Si (100) clearly shows that the Cu (020) has tried to fit with Si (022) by 45 degree rotation in [110] diffraction zone of Si.

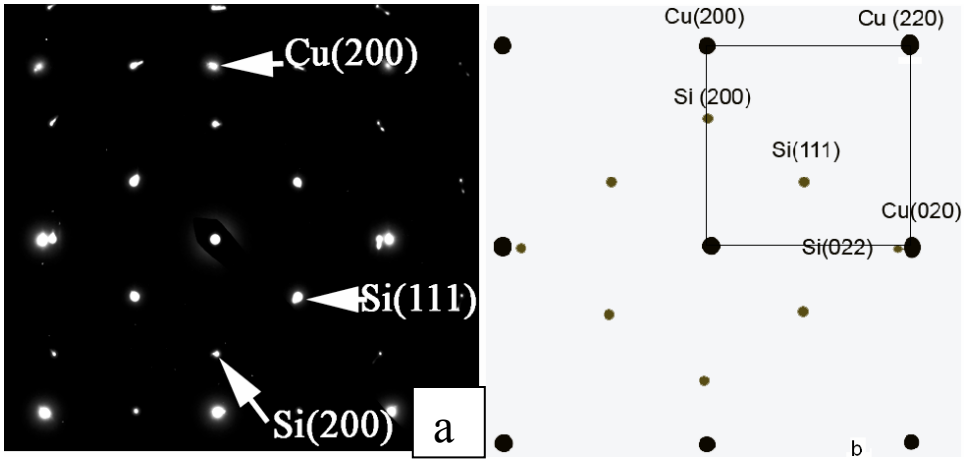

Figure 40 Schematic of diffraction pattern showing the crystal graphic orientations between Cu and Si atomic planes

For Cu deposition on Si (110), one would have thought deposition of Cu (110) with a rotation of 90 degrees with respect to Si (110) would take place as the fractional mismatch becomes 0.057 or 5.7 percent only as clearly seen in figure 41.

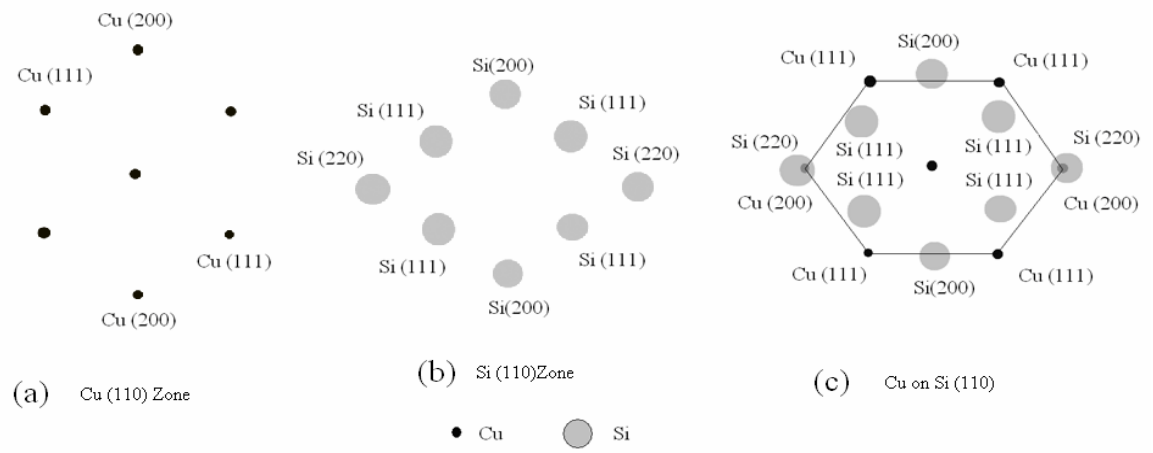

Figure 41 Schematic representation of Cu (110) deposition on Si (110) with a 90 degree rotation

But the X-ray and Transmission Electron Microscope Diffraction pattern show deposition of Cu (111) on Si (110), therefore lattice mismatch should be seen from a completely different angle. 'Invariant line criterion states the optimum matching between two crystal planes at an interface is achieved when there is at least one direction along which the two crystals match perfectly on the interface [73]'. The lattice distance of Si (100) is 0.543, which is just 0.057 times greater than twice the lattice distance of Cu (110) i.e. 0.512 (2 X 0.256) and so taking invariant line criterion in mind it should be possible to grow Cu (111) on Si (110) (figure 44). In diffraction pattern (See figures 42

and 43) of Si [111] zone for Cu (111) on Si (110) the depositing can be clearly understood.

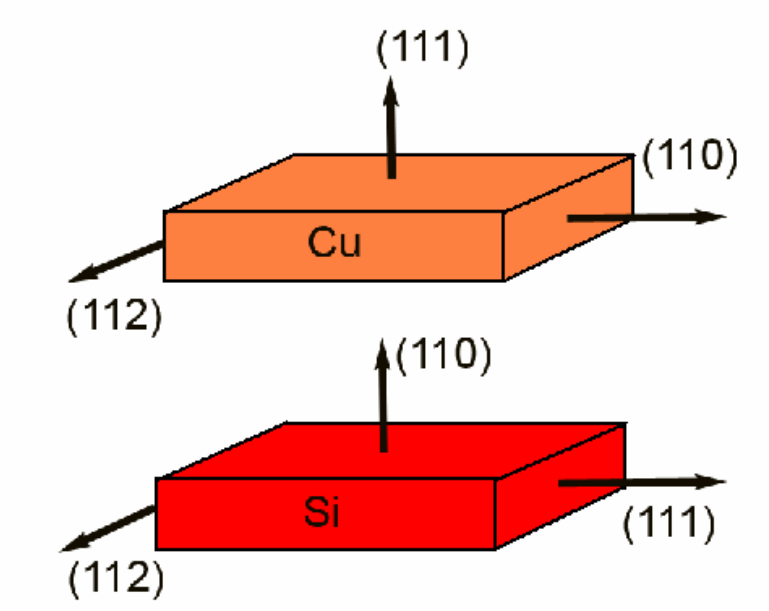

Figure 42 Schematic representation of Cu (111) deposition on Si (110)

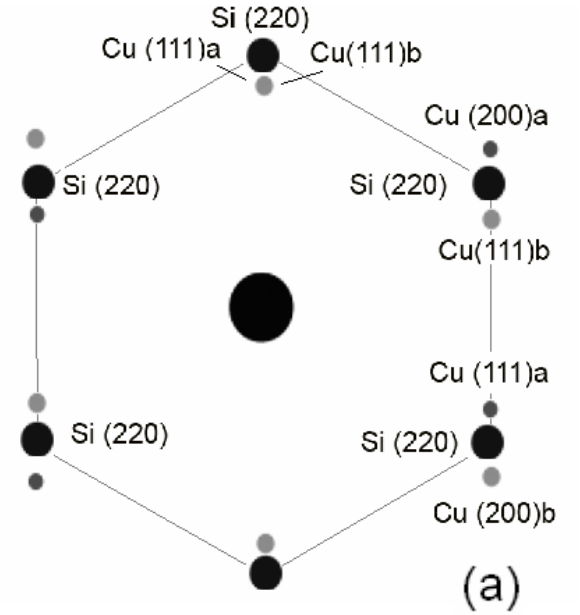

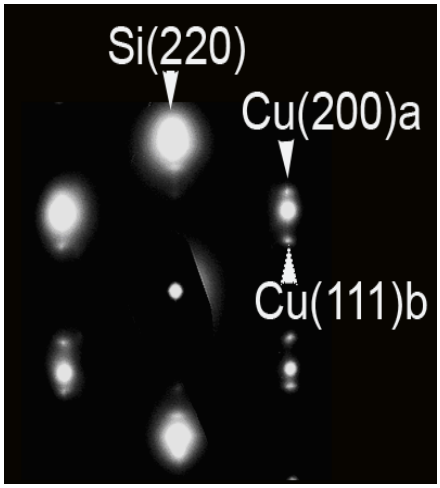

(b)

Figure 43(a) Schematic representation of twin formation of Cu (111) on Si (110) in Si [111] zone, (b) TEM diffraction image of Cu (111)/ Si (110) in Si [111] zone

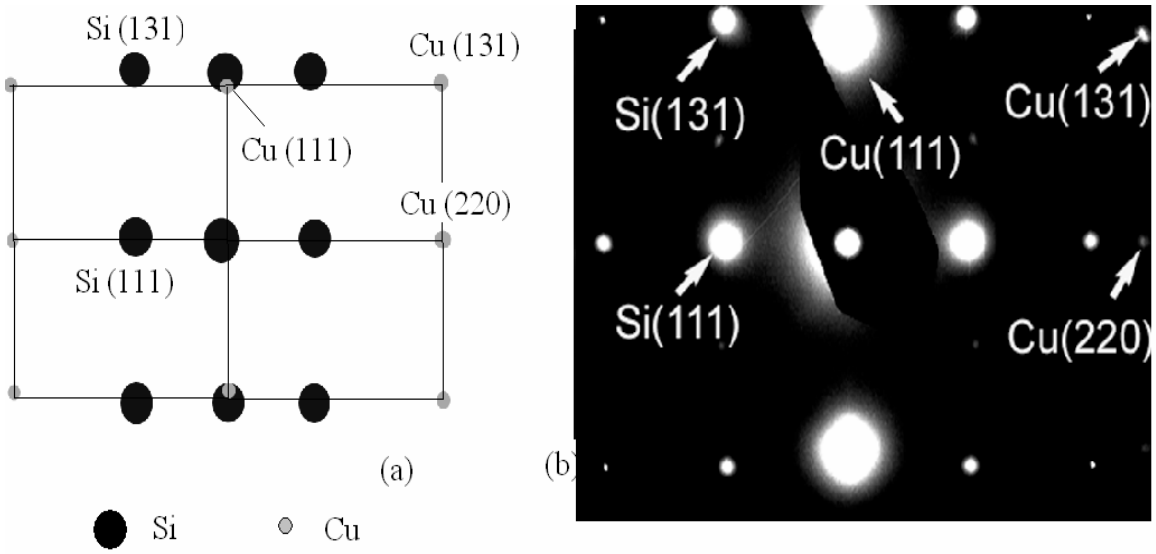

Figure 44(a) Schematic representation of twin formation of Cu (111) on Si (110) in Si [112] zone, (b) TEM diffraction image of Cu (111)/ Si (110) in Si [112] zone

4.1.2 Twin formation in Cu (100) deposited on Si (100)

Along [111] direction, the stacking sequence of (111) planes is ABCABCABC….., but in the case of (100) the stacking sequence is ABABAB…….During the growth of (111) planes, if the film occurs to have 'A' stacking, then the forthcoming atoms can either occupy the parent lattice 'B' or twin lattice 'C' sites. So the subsequent atom which then deposits can either form a normal lattice or twin lattice. But in the case of (100) the subsequent atom can only occupy parent lattice site 'B'. This simple analysis indicates that geometrically twins can not form in Cu (100) single crystal deposited on Si (100) substrate.

4.1.3 Twin formation in Cu (111) on Si (110)

As explained above (111) plane has stacking sequence ABCABCABC….. and if the atom first occupies site ‘A’ then the subsequent atom can deposit at ‘B’ or at faulted site ‘C’, thus it can either form a normal lattice or a twin lattice. The low binding energy difference for atoms that occupy either parent or stacking faulted lattice sites are small (2.567 eV for normal lattice and 2.565 eV for faulted one); this results in easy nucleation of twin domains. Further evolution of domains formed on (111) in [111] direction takes place by lateral expansion of domains. The boundary energy between twin domains is many times larger than that in stacking fault and twin boundary energies, due to which in plane domain boundaries are highly mobile. As a result of less driving force for coarsening in the [111] direction there is layer by layer growth of (111) plane and leads to flat plate like twin structure. Annihilation of these domain boundaries resulted in source for vacancies. On surface this will lead to high surface mobility, whereas if happens in underling layers would cause vacancy trapping [74]. Zhou and Wadley confirmed above discussion with the help of molecular dynamics (MD) simulation of the deposition process

Thermodynamically, the density of growth of twins in sputter deposited Cu can be interpreted in a similar fashion as used for austenitic stainless steel thin films [11]. According to this model:

$$r^{*}_{perfect} = \frac{\gamma}{\left(\frac{kT}{\Omega} \ln\left[\frac{J\sqrt{2\pi mkT}}{P_s} \right] \right)} \qquad (16)$$

$$r^*_{twin} = \frac{\gamma}{\left(\frac{kT}{\Omega}\ln\left[\frac{J\sqrt{2\pi mkT}}{P_s}\right] - \frac{\gamma_t}{h}\right)} \quad (17)$$

where r^* is the critical size of the nucleus (twin and perfect), γ is the surface energy, γ_t is twin boundary energy, k is the Boltsmann constant, T is the substrate temperature, Ω is atomic volume, P_s is vapor pressure of solid, h is the inter-planar thickness, J is the diffusion flux, Usually, $r^*_{perfect} < r^*_{twin}$ and so the nucleation of the perfect nucleus free from twins will be preferred, but from equation: 2 &3 it can be observed that at high deposition rates and low twin boundaries energies the difference comes down to negligible and the twin formation can take place freely

The model further predicts that twinned nuclei will form at rates comparable to defect free nuclei if the free energy change from vapor to solid is comparable to perfect and twinned nuclei. That is, when the deposition material has low stacking fault and twin boundary energies and the deposition rates is high the formation of twins will be preferred. For Cu the stacking fault energy is 45mJ/m^2 and the twin boundary energy is 20mJ/m^2 and the deposition rate is varied from 1nm/sec-2nm/sec which is higher than the one predicted in the model for the formation of twins.

$$\ln\frac{I_{pefect}}{I_{twin}} = \frac{\pi\gamma^2 h\gamma_t}{kT\Delta G_v(h\Delta G_v - \gamma_t)} \quad (18)$$

The process parameters and material properties can be manipulated for provide ways to control the twin densities during the depositions [75, 76].

4.2. Mechanical properties

Nanoindentation tests were conducted on Cu thin films deposited over Si substrates a quantitative analysis of the hardness result is shown in the figure 45. The copper films have much higher hardness than that of the bulk Cu. In figure 45 indentation hardness of bulk copper is depicted by a dashed line and indentation hardness for single crystal Cu (100) and Cu (110) films, and polycrystalline Cu films on SiO_2 are compared. It can be clearly seen that in the case of SiO_2, the hardness increases as a function of deposition power, where as this was not seen in the case of Cu on Si (100) and Si (110). The maximum hardness observed with Cu on SiO_2 is ~2.8 Gpa and 2.5 Gpa in the case of Cu on Si (110)

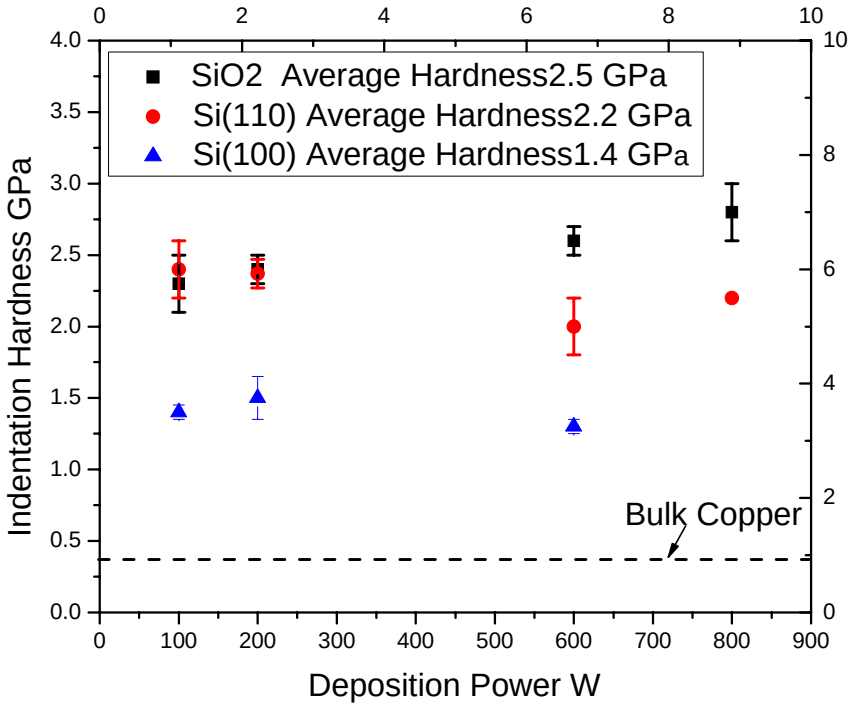

Figure 45 Quantitative analysis of Cu deposited on Si substrates

To understand the difference in film hardness deposited on different Si substrates, we will briefly discuss factors that might affect Cu films hardness, including film thickness dependent hardness, texture dependent and grain boundary dependent harness.

4.2.1. Thickness dependence of hardness

In general finer microstructures attribute partly towards the mechanical properties of thin film. Dislocation density, grain size and film thickness itself can be a huge factor contributing towards hardness. Much of the strength can be attributed to the fact that the substrate constrains dislocation motion in the film. Any oxide layer present on the surface of the film can also constrain the movements of dislocations within the film. According to W.D. Nix there is a linear relation between film thickness and strength, as the thickness decreases the strength increases. But the above relation is true only up to a certain limit. As film thickness increases to over 200nm there is a decrease in the effect of thickness on strength and the film thickness and strength curves reaches a plateau thereafter (See figure 46). Because the thickness of our copper film is 1 to 1.5 μm it is believed that film thickness lie in this plateau region and so the film thickness doesn't play a big role in strengthening these thin films.

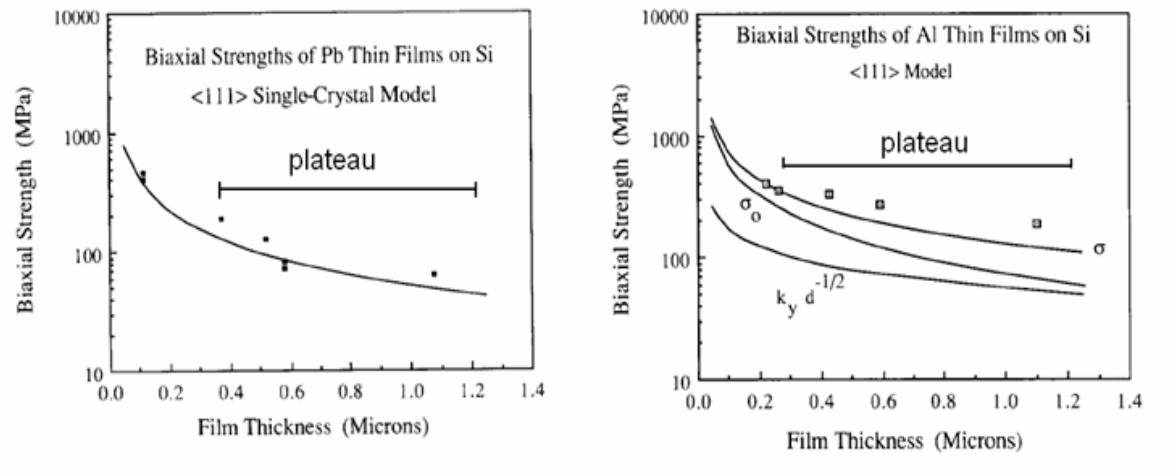

Figure 46 Biaxial strength vs. film thickness graph of Pb/Si and Al/Si [74,77]

4.2.2. Texture dependence of hardness

Anisotropy in the hardness of crystalline minerals has been well established phenomenon. Single crystal metal posses material properties depending on the crystallographic orientation. This anisotropy in the properties of single crystal is related to effective resolved shear stress given by the equation [78]:

$$\tau_e' = \frac{1}{2}\left(\frac{F}{A}\right)\cos\lambda\cos\phi\left(\cos\varphi + \sin\gamma\right) \tag{19}$$

where τ_e is effective resolved shear stress, F is applied force, A is cross-sectional area of specimen, λ is angle between the stress axis and slip direction, Φ is the angle between the stress axis and the normal to the slip plane, φ is the angle between the face of the adjacent facet and the axis of rotation for given slip system, γ is the angle between slip direction and axis parallel to indenter face.

This could be the reason for the extraordinary hardness seen in single crystal copper deposited on Si (100) and Si (110). Biaxial moduli were calculated for Single

crystal Cu (100) and Cu (111) (See table 9). The details of the method used for the calculations can be obtained from reference [79].

Table 9
Single crystal copper and their biaxial modulus

Single Crystal Copper	**Biaxial Modulus**
Cu (100)	115 Gpa
Cu (110)	215 Gpa
Cu (111)	262 Gpa

From nanoindentation tests indentation modulus for all single crystal coppers were calculated as seen in figure 47. These indentation modulus values were found to be approximately the same. Such observation indicates that the observed hardness difference between Cu (100) and Cu (111) films is not because of the texture dependence as well.

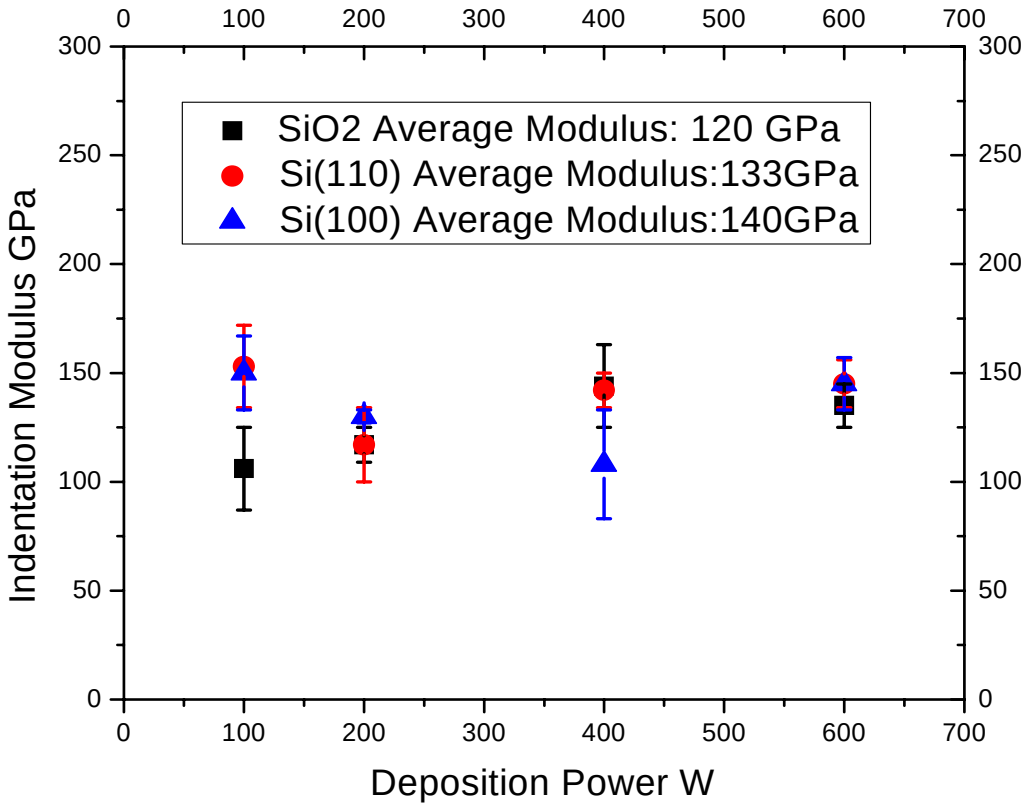

Figure 47 Indentation modulus vs. deposition power plot for Cu on Si substrates

4.2.3. Grain-size reduction induced hardness

Grain boundaries have proved to be a strong barrier to the motion of dislocations. This is because different gains in neighborhood have different orientations. And so to cross the grain boundary dislocations have to change the direction of motion and with in a grain boundary region due to atomic disorder there is discontinuity of slip planes from one grain to another. Grain size dependent hardness is not applicable in this study because XRD analyses clearly depict that the Cu (100) and Cu (111) thin films are single crystal in nature (See figures 20 & 21), whereas in Cu on SiO_2 the grain size is too large (micrometer range as seen in figure 48, to create such high strength (2.2-2.5 Gpa) in polycrystalline Cu films.

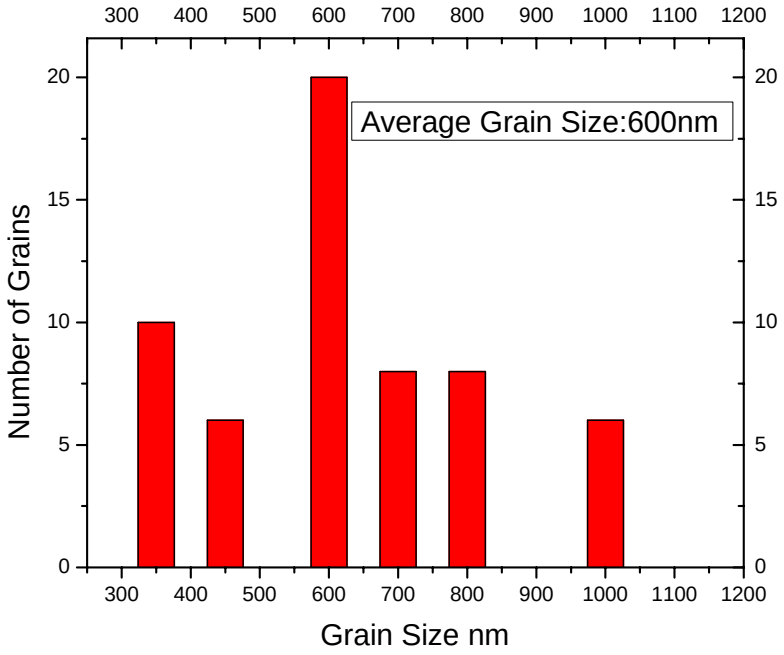

Figure 48 Statistical result form TEM for average grain size of Cu on SiO_2

4.2.4. Nanoscale twinning induced hardness

Twinnings are defined as a type of boundary across which there is specific mirror lattice symmetry [22]'; that is atoms on both sides of the boundary are mirror image of each other.

4.2.4.1. Cu (111) on Si (110)

As the influence of impurities, density, Average grain-size and texture can be ruled out for contributing to extraordinary hardness, the variation in strength can be solely attributed to Twin boundaries. Twin boundaries have proven to have an equivalent effect on the strength of materials as grain boundaries. Hall-petch governed strengthening was witnessed in α-brass with grain boundaries in the range of tens of micrometer, where twin spacing was the main governing factor in strengthening [80]. The interaction of glide dislocation with twin boundary affects immensely the mechanical property of thin film. It is indicated that the propagation of slip bands are blocked by these twin defects.

It is seen that twin boundaries are very strong obstacles to transmission of glide dislocations. Though Dislocations can pile-up and transfer across the twin boundary due to stress concentrations at twin slip band intersections, but dislocation pile ups form at high lamellae thickness, with twins spaced at nanometer range the strength is said to dependent on single dislocation motion across twin boundary. Thus, by decreasing the twin spacing to nanometer range the tensile strength can in increased by many folds [81]. Higher the twin boundary density- higher is the capacity of dislocation accumulations, leading to enhanced strengthening.

Statistical measurement of the twin thickness and spacing over several samples of Cu (111) on Si (110) deposited at 800W indicated that the twin thickness in one batch or samples is 20nm and spacing of same order 20 nm, and the twin thickness in other batch was 10nm and spacing 5nm (See figures 49 (a), (b), (c), (d)). The variation in the twin spacing is suspected to the heating effect in earlier samples. Further studies are underway in our laboratory to understand how to tailor twin spacing experimentally.

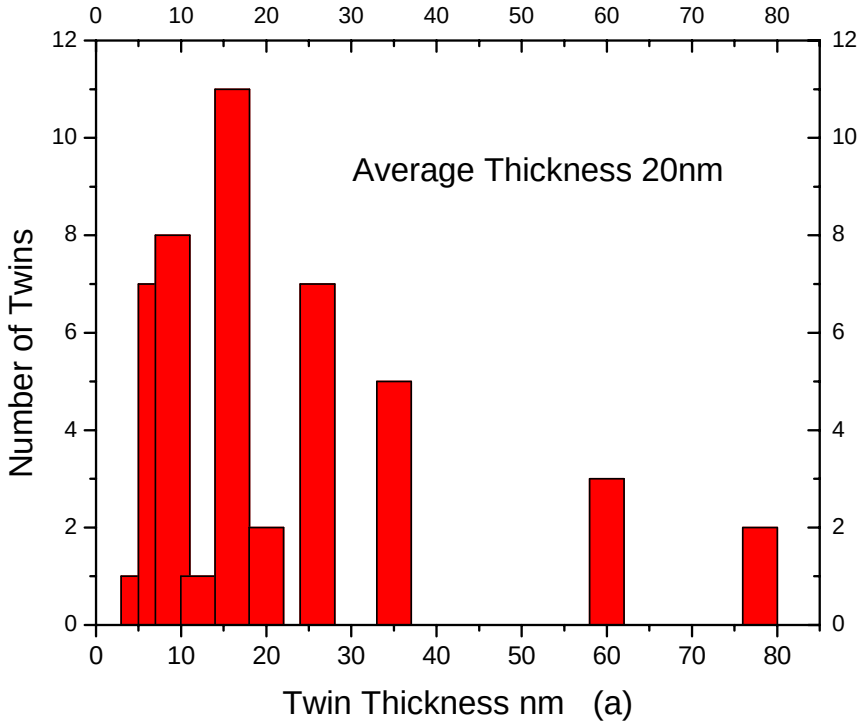

Figure 49 Statistical result from TEM images show that (a) Average twin thickness for Cu(111) sample deposited with heating affect is 20nm and (b) Average twin spacing is 20nm, whereas (c) Average twin thickness for Cu (111) sample deposited without heating affect is 10nm and (d) Twin spacing is 5nm

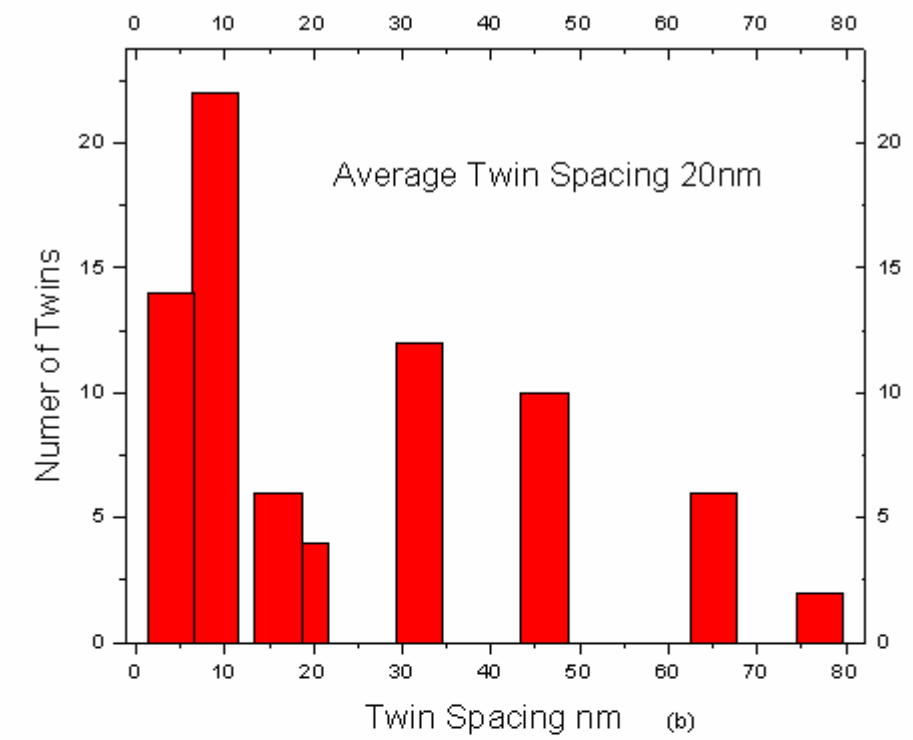

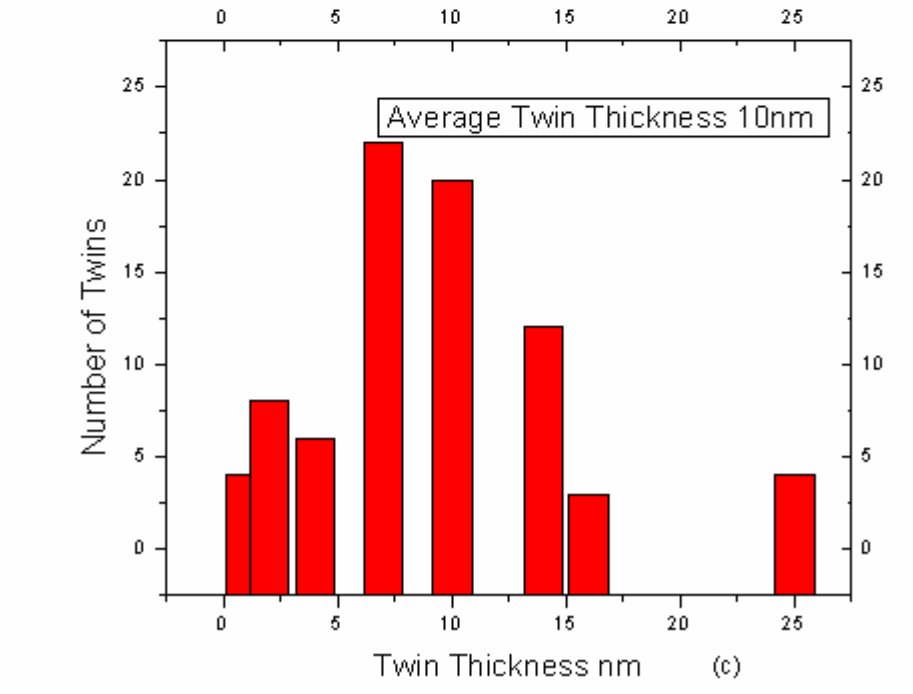

Figure 49 Continued

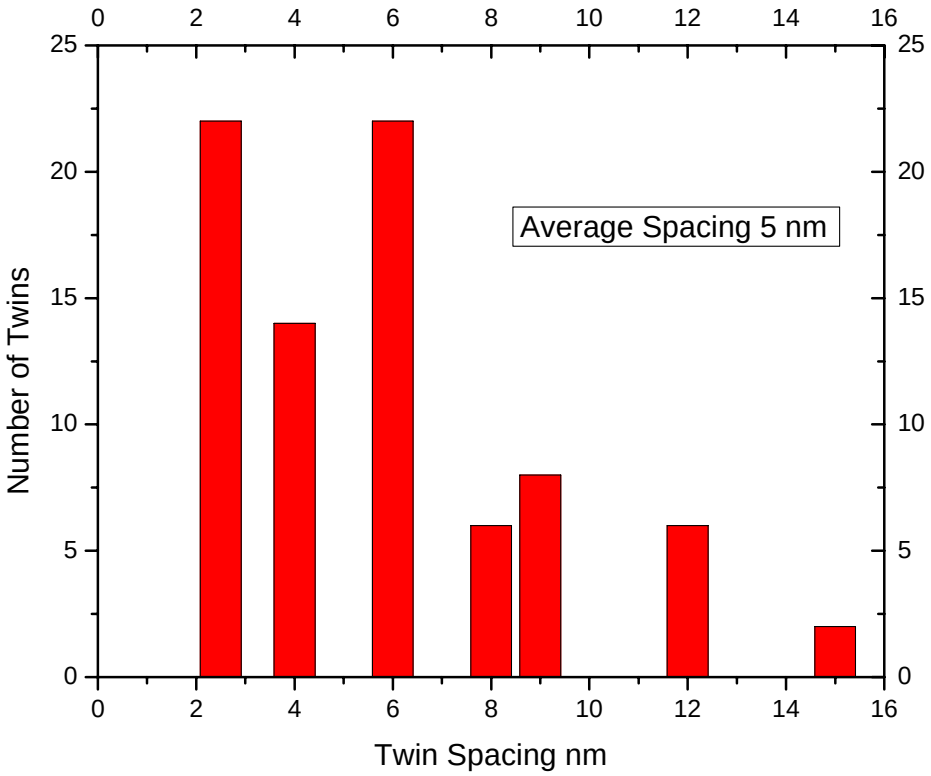

Figure 49 Continued

It is clear from above statistical data that the former Cu (111) on Si (110) had twin thickness and twin spacing much less than the later mentioned Cu (111) on Si (110) samples. In order to prove that twin boundary is the sole reason for the high strength nanoindentation test was done on the later Cu (111) on Si (110) samples (See figure 50)

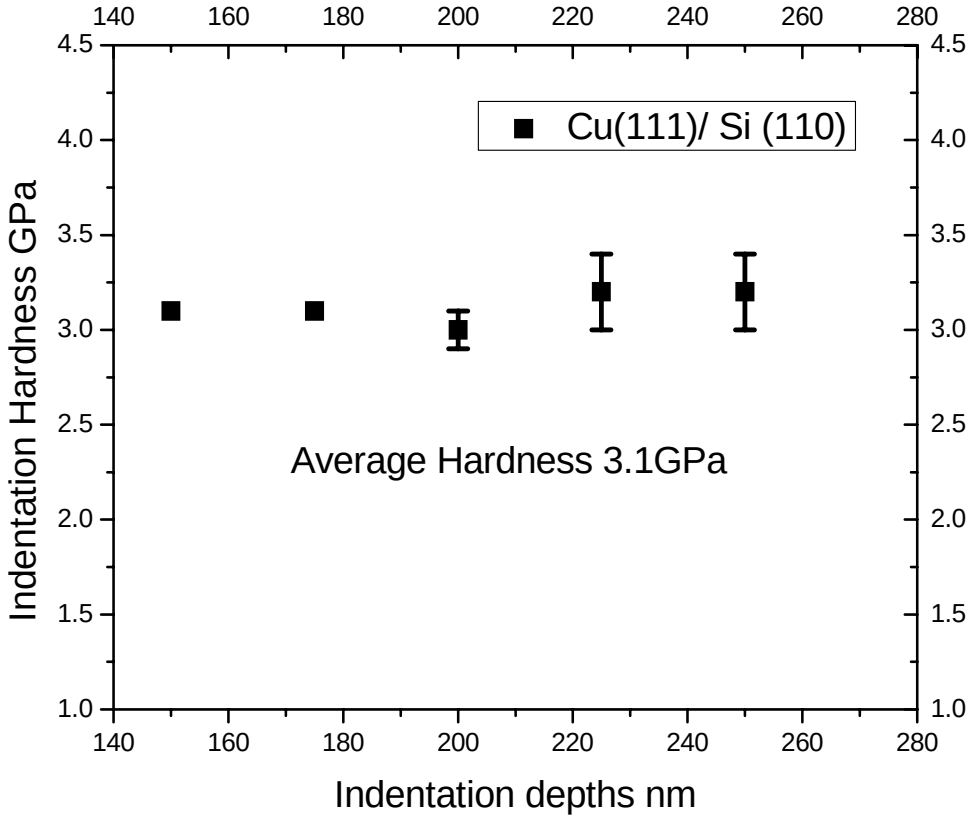

Figure 50 Indentation hardness vs. indentation depth plot for Cu (111)/Si(110) without heating effect

It was seen that the hardness of Cu (111) on Si (110) with twin thickness and spacing has hardness of 3.1 GPa, which is about 1 GPa higher than the sample with twin thickness and spacing about 10nm and 20 nm. And confirms our hypothesis that the extraordinary strength of Cu (111) on Si (110) is solely due to the high density twinning and as the twin density increases the hardness also increases (See figure 51 & 52).

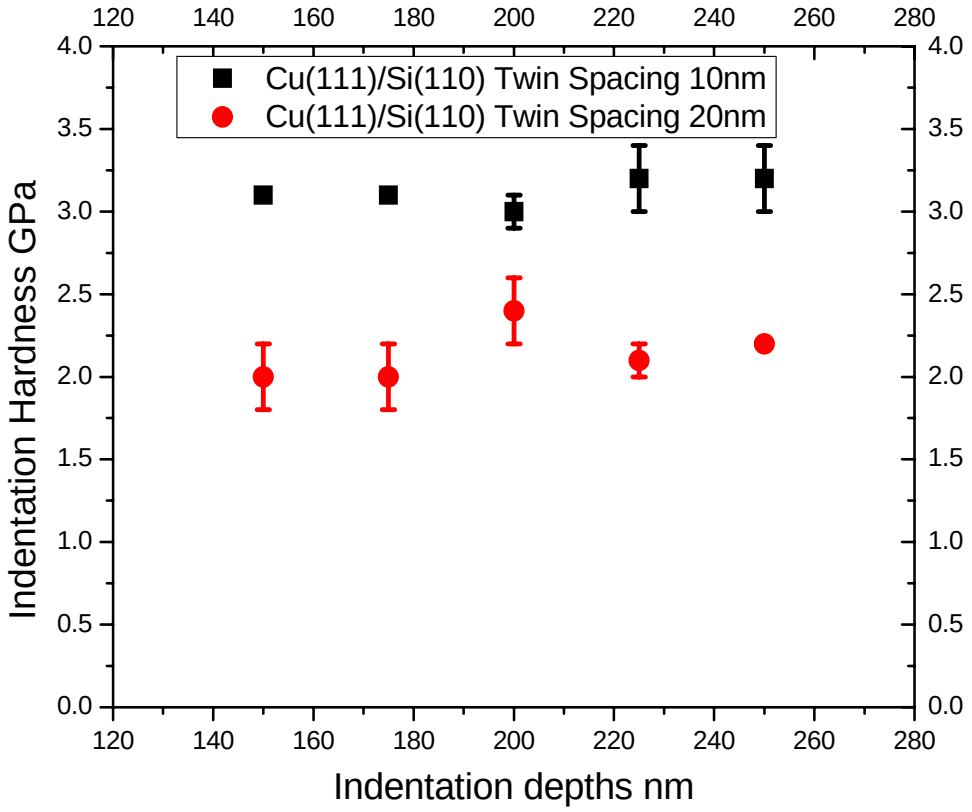

Figure 51 Indentation hardness vs. indentation depths plots for Cu(111) on Si (110) with different twin spacing

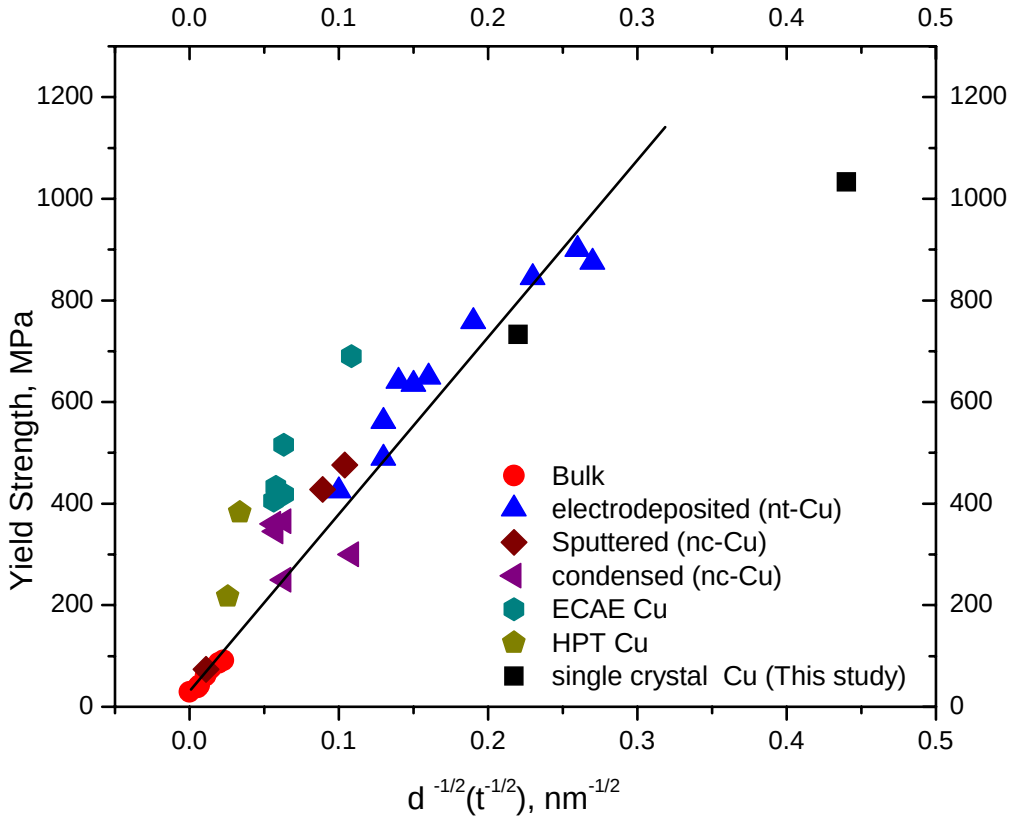

Figure 52 Yield strength vs. inverse displacement for different types of copper thin film [47-50, 82].

Above plot gives a comparative picture of all the different hardened copper obtained by various techniques. The hall-petch hardening is presented by the line. Literature review shows that all the coppers as they get hardened loose conductivity and so the copper with yield strength around 800 MPa have very high resistivity. The resistivity study for copper deposited in this study is discussed in electrical property section.

4.2.4.2. Cu on SiO_2

As seen from XRD results the Cu films on SiO_2 is polycrystal in nature with dominant grain orientations of (111). The average grain size seen in the plan view samples were about 600nm (See figure 48). Further, there was a presence of high density of twins at present at an angle. In Statistical measurement from a number of plan view TEM graphs it was confirmed that the average twin spacing and thickness of these twins is ~50 nm (See figures 53 and 54).

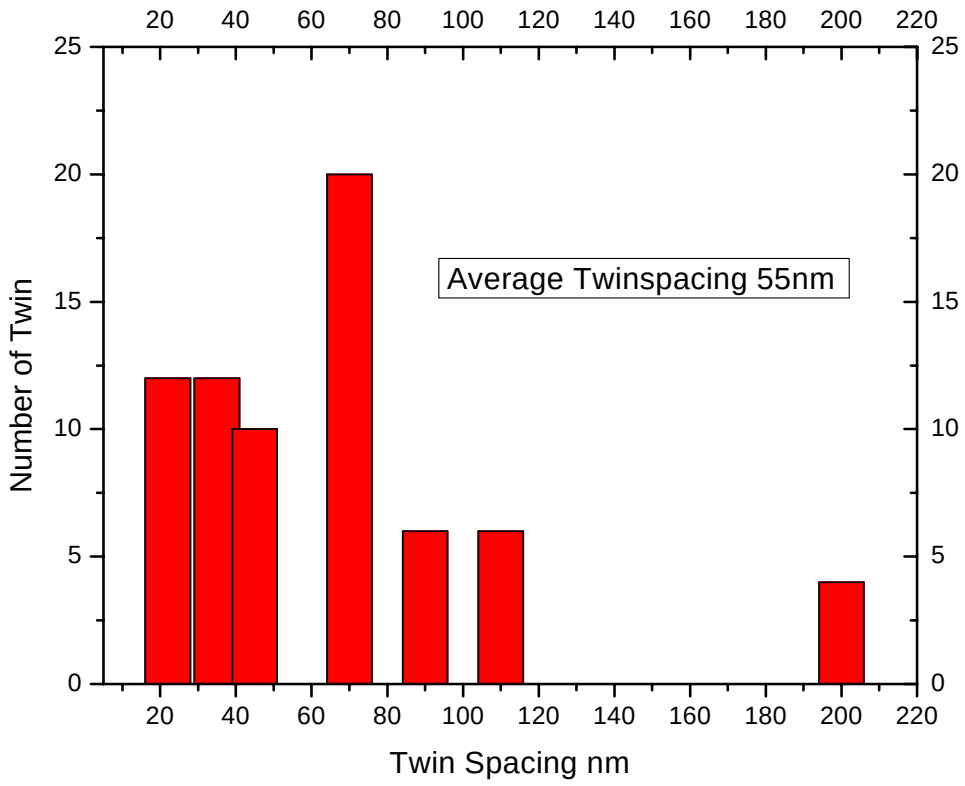

Figure 53 Statistical data from TEM results showing that the average of twin intercepts on horizontal plane in Cu on SiO_2 is 50 nm

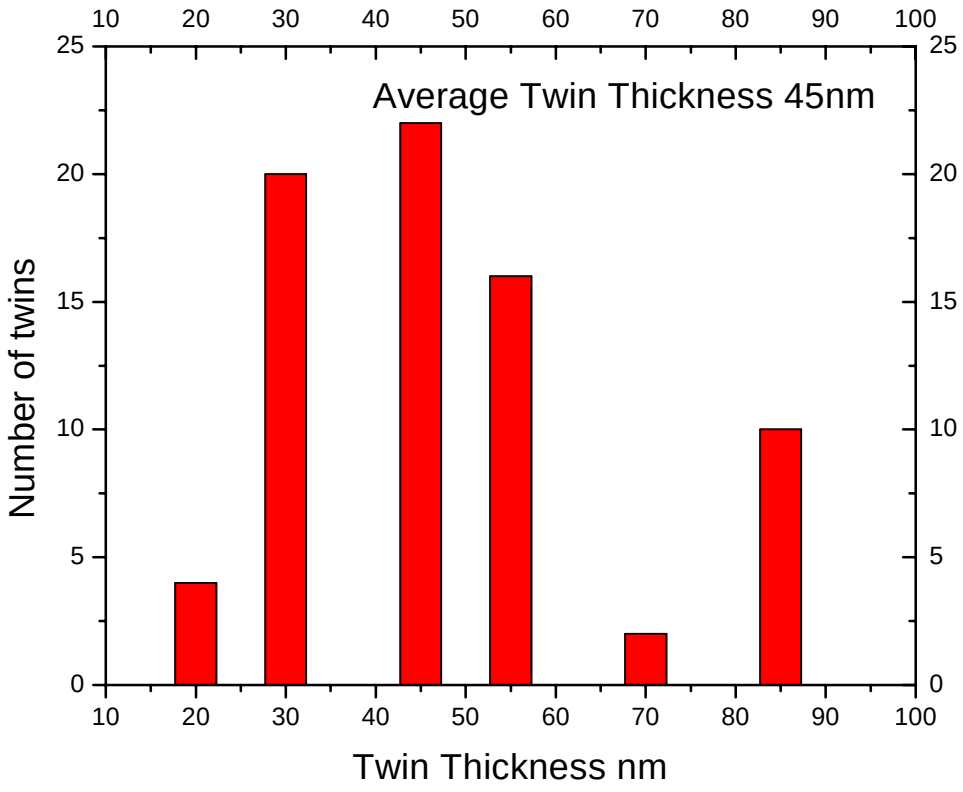

Figure 54 Statistical data from TEM results showing that the average of twin thickness in Cu on SiO_2 is 45 nm

It has been already a proven fact that twin densities play an important role in the mechanical properties of the material [75, 76, and 81]. In polycrystal films as the density of twins decreases the yield strength of the metal has been seen dropping. It is known that when glide dislocation come in contact with the twin boundary in side the grain, the dislocation glide will encounter high density of twin boundaries. These dislocations can also pile up and propagate across the twins, if they went dislocation dissociation reaction, which will require stress concentrations at twin slip band intersection giving us the improved strength.

Summarizing, it is clearly seen that in Cu (111) on Si (110) and Cu on SiO_2, the high hardness was not caused by grain–size reduction, texture effect or by thickness reduction. And these aspects had a negligible effect on the hardness of these sputter deposited films. The high density twin boundary have proved to be very effective barrier to the dislocation motion and as their density increases the hardness increases, so twin boundaries can be considered to be the sole reason for the high hardness observed in the Cu films.

4.3. Electrical properties

It is seen that as the temperature increases the resistivity increases, it is known that as the temperature rises there is increase in the thermal vibrations and lattice irregularities, these vibrations and irregularities act as electron scattering centers causing the resistivity increases. At room temperature (298 K) the resistivity measurement for Cu (100) in Si (100) was 1.95 ± 0.02μΩ·cm, for Cu (111) on Si (110) the resistivity is 2 ± 0.02 μΩ·cm and for Cu on SiO_2 the resistivity is1.90 ± 0.02 μΩ·cm. The resistivity of coarse grained copper is reported to have resistivity of 1.67±.01 μΩ·cm which is just a fraction lower than the resistivity reported by copper in this study as shown in Figure 55.In comparison copper with similar hardness are nanocrystalline copper, it is already a fact that grain boundary are effective electron scattering site and as the number of grain boundaries increase the resistivity also increases. These copper have reported a resistivity value or about 18±1 μΩ·cm which is at least one order of magnitude higher that nano-twinned Cu in this study [81]. Therefore the current studies indicate that growth twins may provide barriers for dislocation transmission, but not interfering with electron trespassing. Therefore by design metallic materials with high density twins might be a promising approach in achieving high-strength and high conductivity.

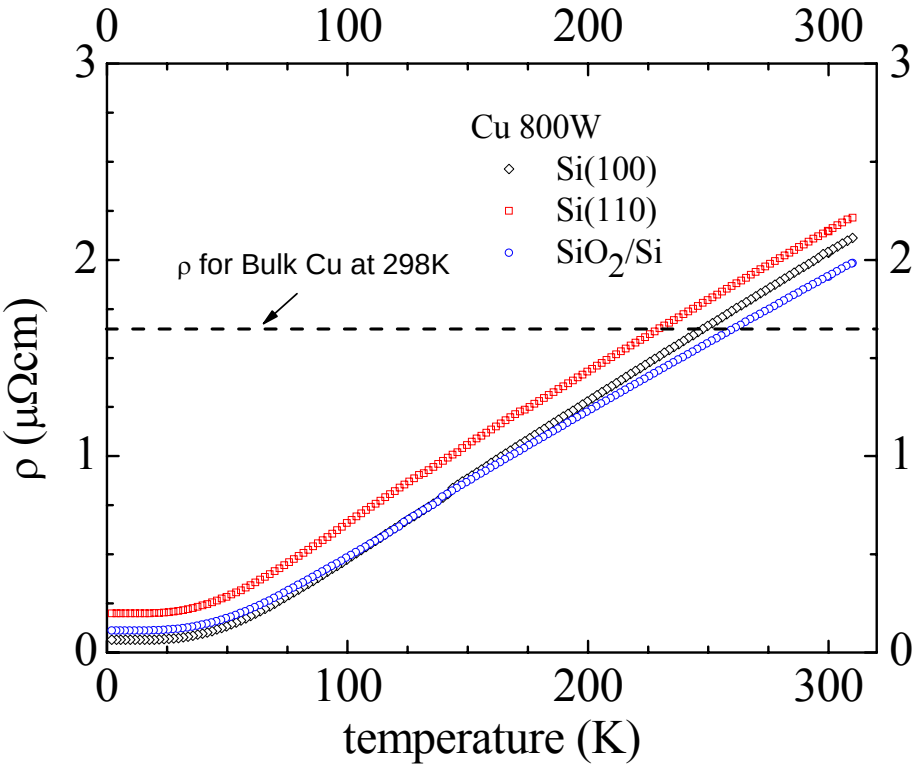

Figure 55 Resistivity vs. temperature plot for Cu (111) on Si (110) deposited at 800W

5. CONCLUSION

Sputter deposition is one of the best techniques for the deposition of Cu thin films free from intermixing with substrate at room temperature. Cu thin films were sputter-deposited onto Si (100), Si (110) and SiO_2 substrates. Epitaxial growths of Cu (100) on Si (100) substrate, and Cu (111) on Si (110) substrate were observed via XRD and TEM studies. TEM studies also reveal high density of {111} type growth twins in single crystal Cu (111) grown on Si (110) substrates. Grow twins oriented parallel to substrate surfaces with twin spacing of a few or tens of nanometers. Our thermodynamic model indicates that since twin boundary energy of Cu is small, at higher deposition rates, high density growth twins can be induced. Nanoindentation studies show that Cu films with high density growth twins have very high hardness, 2-2.5 GPa. Such studies indicate that twin boundaries can act as strong obstacles to the transmission of dislocations, in a similar fashion as grain boundaries. Electrical resistance of high-strength, nanotwinned single crystal Cu films is similar to that of conventional bulk Cu. This project indicates that twin boundaries may provide a very effective approach in producing high strength and high electrical conductivity metallic materials.

6. FUTURE WORK

From this study it was proven that twin density plays an important role in enhancing mechanical properties of Cu thin films while maintaining low electrical resistivity of metals.

- Deposition condition seems to play a very important role in twin formation in Cu thin films. Further studies will focus on understanding the effects of deposition parameters on the formation of growth twins.
- The thermal stability of these twin boundaries is unknown. So further studies will involve the understanding of thermal stability of these twin boundaries and compare such studies with the thermal stability of grain boundaries in nanocrystalline Cu.
- Ni has the same crystal structure as that of Cu, with however a much higher stacking fault energy. We will investigate the sputter-deposited Ni films to gain knowledge about the formation of growth twins in Ni, and the influence of the twin density in increasing the mechanical strength of Ni films.

A comparison between the contemporary studies and current studies is shown in figure 56. A similar range of hardness value obtained by the synthesis of Cu with nanocrystalline grains leads to a resistivity value around 18 μΩ·cm, whereas in this study the Cu deposited has resistivity value of ~1.9 μΩ·cm. We will attempt to deposit Cu films with hardness value of 4 GPa or higher by inducing higher density of growth twins, while maintaining resistivity value in near vicinity of 1.9 μΩ·cm.

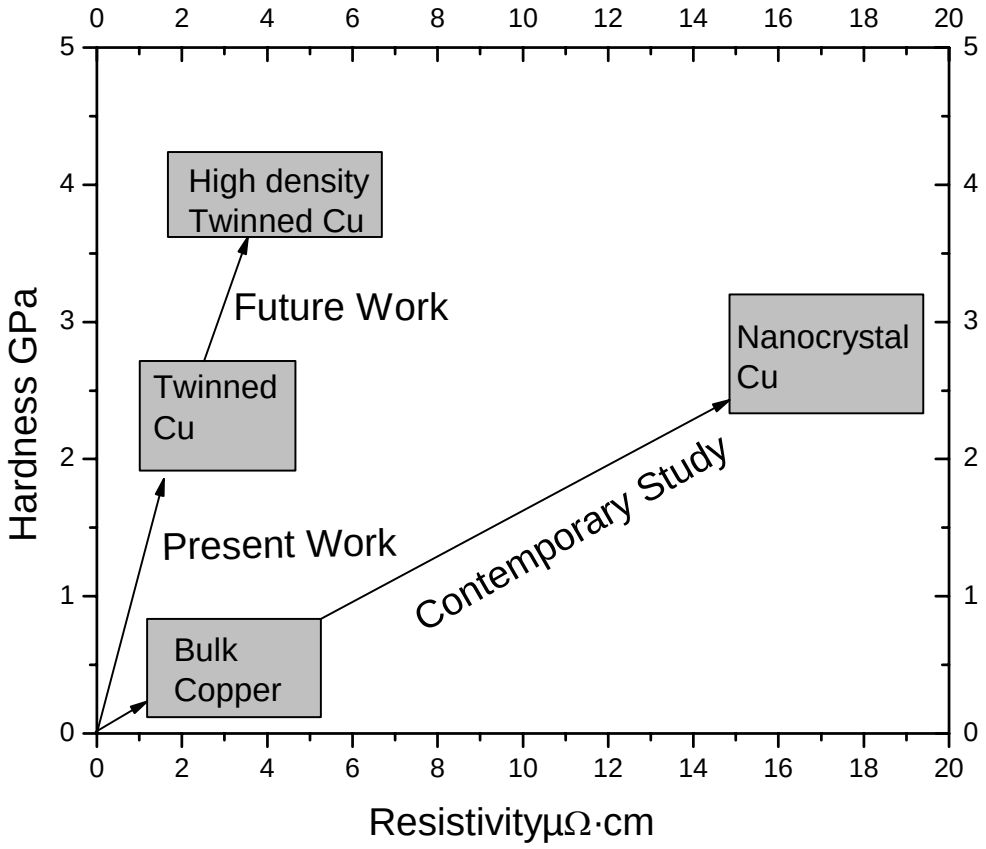

Figure 56 Schematic representation of present and future work

REFERENCES

[1] "Thin Film" Wikipedia Encyclopedia, http://en.wikipedia.org/wiki/Thin_films: 06/11/07.

[2] Smith D. Thin film deposition: principles and practice. New York: McGraw-Hill, Inc; 1995.

[3] Wagner T. Thin film science. Stuttgart, Germany: Max-Planck-Institute for Metalliforchung.

[4] Siegel R. W, Hu E. H, Roco M. C, WTEC panel report on R & D status and trends in nanoparticles, nanostructured materials, and nanodevices. Boston: Kluwer Academic Publishers; 1997.

[5] Kumar A, Chung Y.W, Moore J. J, Smugeresky J. E. Surface engineering, science and technology I. Warrendale(PA): The Minerals, Metals &Materials Society; 1999 . p. xi+513.

[6] Kumar A, Chung Y.W, Chia R. W. J, Hard coatings. Warrendale (PA): The Minerals, Metals & Materials Society 1998. p. x+394.

[7] Brookhaven national laboratory. Growth and processing of advanced materials. http://www.bnl.gov/nsls2/sciOps/chemSci/growth.asp: 06/06/07.

[8] Barlow F, Elshabini-Riad A, Brown R. Film deposition techniques and processes. New York: McGraw Hill; 1998.

[9] Mattox D M. Handbook of physical vapor deposition (PVD) Processing. New York: William Andrew Inc; 1998.

[10] Robin F.C. Molecular beam epitaxy: applications to key materials; New York: William Andrew Inc; 1995.

[11] Wasa K, Kitabatake M, Adachi H. Thin film materials technology: sputtering of compound materials. New York: William Andrew Inc; 2004.

[12] Hitchman M.L, Jensen K.F. Chemical vapor deposition: principles and applications. New York: Academic Press Ltd; 1993.

[13] Tracy D.P, Knorr D.B. Texture and microstructure of thin Cu films, Journal of Electronic Materials 1993; 22:611-16.

[14] Ohmi. T, Tsubouchi K. Advanced copper metallization technology for ULSI interconnects. Solid State Technology 1992; 35: 47-52.

[15] Li Jian, Mayer J.W, Colgan E.G. Oxidation and protection in copper and copper alloy thin films, Journal of Applied Physics 1991; 70:2820-7.

[16] Zhou J.B, Gustafsson T. Growth of thin Cu films on MgO (001), Surface Science 1996; 375:221-5.

[17] Vossen L J, Kern W. Thin film formation, Physics Today 1980; 33:26.

[18] E.V. Barnat, D.Nagakura, P.I.Wang, T.M.Lu. Real time resistivity measurements during sputter deposition of ultrathin copper films, Journal of Applied Science 2002; 91:1667-72.

[19] Kah-Yoong C, Bee-San T. Atomic force microscopy and X-ray diffraction investigations of copper thin films prepared by dc magnetron sputtering technique, Microelectronics Journal 2006;37:1064-71.

[20] Ektessabi A.M. Temperature dependence of atomic mixing of the copper silicon interface, Thin Solid Films 1993; 236:135-9.

[21] Venables J. Introduction to surface and thin film processes, Cambridge: Cambridge University Press 2000.

[22] Callister W.D, Jr. Material science and engineering: an introduction. New York: John Wiley & Sons, Inc 1997.

[23] Otooni M.A. A new technique for preparation of single crystal copper; Journal of Crystal Growth 1979; 46:209-12.

[24] Purswani J.M, Spila T, Gall D. Growth of epitaxial Cu on MgO(001) by magnetron sputter deposition. Thin Film Solids 2006; 515:1166-70.

[25] Brockway L.O, Marcus R. B. Microstructure of thin single crystals of copper. Journal of Applied Physics 1961; 34:921-923.

[26] Matthews J. W, Crawford J.L. Accommodation of misfit between single crystal films of nickel and copper, Thin Solid Films 1970; 5:187-98.

[27] Bialas H, Heneka K. Epitaxy of fcc metals on dielectric substrates. Vacuum 1992; 45:79-87.

[28] Swankt T.F, Lawless K.R. Catalysis on thin single crystal copper films, Journal of Applied Physics 1964; 36: 2089-2090.

[29] Jiang H, Klemmer T.J, Barnard J.A, Doyle W.D, Payzant E.A. Epitaxial growth of Cu (111) films on Si (110) by magnetron sputtering: orientation and twin growth, Thin Solid Films 1997; 315:13-16.

[30] Macur J.E, Vook R.W. Initial epitaxial growth of (111)Au/(111)Cu and (111)Cu/(111)Au, Thin Solid Films1979;66:371-9.

[31] Feder J, Rudole P, Wissmann P. The resistivity of single crystal copper films, Thin Solid Films 1975; 31:183-6.

[32] Liu C.S, Chen S.R, Chen W.J, Chen L.J. Epitaxial growth of Cu thin films on atomically cleaned (111) Si at room temperature. Material, Chemistry and Physics 1993; 36:170-3.

[33] Hull D. Introduction to dislocations. New York: Pergamon Press, Inc. 1984

[34] Read W.T. Jr. Dislocations in crystals. New York: McGraw Hill Book Company 1953.

[35] The Hall-Petch relationship. http://www.matsci.ucdavis.edu/MatSciLT/EMS-174L/Files/HallPetch.pdf. 06/06/07.

[36] Hall E.O. The deformation and ageing of mild steel. II. Characteristics of the Luders deformation, Proceedings of the Physical Society 1951; B64:747.

[37] Petch N.J. The cleavage strength of polycrystal, Journal of the Iron and Steel Institute 1953;174:25.

[38] Goddard A.W. Handbook of nanoscience, engineering and technology, London: CRC Press 2003.

[39] Schiotz J, Tolla F.D Di, Jacobsen K.W. Softening of nanocrystalline metals at very small grains. Nature 1998; 391:561.

[40] Giga A, Kimoto Y, Takigawa Y, Higashi K. Demonstration of an inverse Hall–Petch relationship in electrodeposited nanocrystalline Ni–W alloys through tensile testing, Scripta Materialia 2006; 5:143-6.

[41] Fan G.J, Chooa H, Liawa P.K, Lavernia E.J. A model for the inverse Hall–Petch relation of nanocrystalline materials. Materials Science & Engineering 2005; 409:243-8 .

[42] Hosford F W. Mechanical behavior of materials, Cambridge: Cambridge University Press; 2005.

[43] Kodgire V.D. Material science and metallurgy. Maharashtra (India): Everest Publication House; 2002.

[44] Siow K.S, Tay A.A.O, Oruganti P. Mechanical properties of nanocrystalline copper and nickel. Material Science and Technology 2004; 20: 285-294.

[45] Merz M.D, Dahlgren S.D. Tensile strength work hardening of ultrafine grained high purity copper. Journal of Applied Physics 1975; 46:3235-7.

[46] Chen J, Lu L, Lu K. Hardness and strain rate sensitivity of nanocrystalline Cu. Scripta Materialia 2006;54:1913-18.

[47] Jiang H, Zhu Y. Theodore, Butt D. P, Alexandrov I.V, Lowe T.C. Microstructural evolution, microhardness and thermal stability of HPT-processed Cu. Material Science and Engineering 2000; A290:128-38.

[48] Meyers M.A, Mishra A, Benson D.J. Mechanical properties of nanocrystalline materials, Progress in Material Science 2005; 51:427-556.

[49] Xiang Y, Tsui T.Y, Vlassak J.J. The mechanical properties of freestanding electroplated Cu thin films. Materials Research Society 2005; 21:1607-18.

[50] Gertsman V.Y, Hoffmann M, Gleiter H, Birringer R. The study of grain size dependence of yield stress of copper for a wide grain size range. Acta Materialia 1993; 42: 3539-44.

[51] Nix W D. Mechanical properties of thin films. The Minerals, Metal and Materials Society 1989; 20A:2217-45.

[52] Choi Y, Subra S. Size effect on the mechanical properties of thin polycrystalline metals films on substrates, Acta Materialia 2002; 50: 1881-1893.

[53] Lu L, Shen Y, Chen X, Qian L, Lu K. Ultra high strength and high electrical conductivity in copper. Science 2004; 304:422-26.

[54] Keller R.M, Baker S.P, Arzt E. Quantitative analysis of strengthening mechanisms in thin Cu films: effects of film thickness, grain size, and passivation, K.Mater.Res.1998;13:1307-17.

[55] Ehrenreich H. Electrical properties of materials, Scientific American. 1967; 217: 195-209.

[56] Agarwal B.K. X-ray Spectroscopy: an introduction. New York: Springer-Verlag.1991.

[57] Bragg W.L. The diffraction of short electromagnetic waves by a crystal, Proceedings of the Cambridge Philosophical Society 1912;17:43–57.

[58] Abrahams M.S, Buiocchi C.S. Cross-sectional specimens for transmission electron microscopy. Journal of Applied Physics 1974; 45: 3315-16.

[59] Thomas G, Goringe J.M. Transmissiont electron microscopy of materials. New York: John Wiley and Sons.1979.

[60] Bach H, Schroder H. Electron microscopic investigation of transverse sections of thin films on solid substrates, Zeitschrift fur Physik A (Atoms and Nuclei) 1969; 224:122-5.

[61] Williams D B, Carter B. Transmission Electron Microscope, New York: Plenum Press 1996.

[62] Bozzola J.J, Russell L.D. Electron microscopy: principle and technique for biologists. Boston: Jones & Bartlett Publishers 1999.

[63] Tabor D. Indentation hardness: fifty years on a personal view; Philosophical Magazine A 1996; 1207-1212.

[64] Bangert H, Kaminitschek A, Wagendristel A, Darna A, Darna P.B, Radnoczi G. Ultramicrohardness measurements on aluminum films evaporated under various conditions. Thin Solid Films 1896; 137:193-198.

[65] Hannula S.P, Stone D, Li C. Y. Determination of time-dependent plastic properties of metals by indentation load relaxation techniques. Electronic packaging materials science. Materials Research Society Symposia Proceedings 1985; 40:217-224.

[66] Stone D, LaFontaine W.R, Alexopoulous P, Wu T. W, Li C. Y. An investigation of hardness and adhesion of sputter-deposited aluminum on

silicon by utilizing a continuous indentation test. Journal of Materials Research 1988; 3:141-147.

[67] Pethica J.B, Oliver W.C. Mechanical properties of nanometre volumes of material: use of the elastic response of small area indentations. Materials Research Society Symposia Proceedings 1989; 130:13-32.

[68] Metallic materials: instrumented indentation test for hardness and materials parameters. International Organization for Standardization. 2002; 14577-1.

[69] Baker S.P, Burnham N. Measuring mechanical properties in the nanometer regime. Thin Solid Films.1997; 308-309:289-96.

[70] W.C. Oliver, G.M. Pharr. An improved technique for determining hardness and elastic modulus using load and displacement sensing indentation experiments. Journal of Material Research 1992; 7:1564-83.

[71] Anantha N.G, Bhatia H.S, Cavaliere J.R. Four-point probe contact resistivity measurement. IBM Disclosure Bulletin 1979; 21: 3216.

[72] Smith D L. Thin film deposition: principles and practice, New York: McGraw-Hill Publications 1995.

[73] Kato M, Wada M, Sato A, Mori T. Epitaxy of cubic crystals on (001) cubic substrates. Acta Metallurgica 1989; 37:749-56.

[74] Jiang H, Klemmer T.J, Barnard J.A, Doyle W.D, Payzant E.A. Epitaxial growth of Cu (111) films on Si (110) by magnetron sputtering: orientation and twin growth. Thin Solid Films 1997; 315:13-16.

[75] Zhang X, Mishra A, Wang H, Shen T.D, Nastasi M, Mitchell T.E, Hirth J.P, Hoagland R.G, Embury J.D. Enhanced hardening in Cu/330 stainless steel multilayers by nanoscale twinning. Acta Materialia 2003; 52: 995-1002.

[76] Zhang X, Wang H, Chen X.H, Lu L, Lu K, Hoagland R.G, Mishra A. High strength sputter deposited Cu foils with preferred orientation of Nanoscale growth twins. Applied Physics Letters 2006; 88: 173116-1-3.

[77] Doerner M.F, Gardner D.S, Nix W.D. Plastic properties of thin films on substrates as measured by submicron indentation hardness and substrate curvature techniques. Journal of Material Research 1986; 1:845-851.

[78] Brookes C.A, O'Neil J.B, Redfern B.A.W. Anisotropy in the hardness of single crystals. Proceedings of the Royal Society of London 1971; 322:73-88.

[79] Huang F, Weaver M. L. Biaxial modulus of fiber-textured cubic polycrystalline films with an arbitrary texture axis [hlk]. Journal of Applied Physics 2005; 98:073505-1-6.

[80] Kuan T.S, Murakami M. Low-temperature strain behavior of Pb thin films on a substrate. Metallurgical Transactions 1982; 13A:383-91.

[81] Shen Y.F, Lu L, Lu Q.H, Jin Z.H, Lu K. Tensile properties of copper with nano-scale twins. Scripta Materialia 2005; 59: 989-94.

[82] Legros M, Elliott B.R, Rittner M.N, Weertman J.R, Hemker K.J. Microsample tensile testing of nanocrystalline metals. Philosophical Magazine 1999; 80: 1017-26.

VITA

Name: Vibhor Vinodkumar Jain

Address: 5509 Lindsey Drive, Plano, Texas 75093

Email Address: vibhorjain82@tamu.edu

Education: Bachelors of Engineering, Production Engineering, Shivaji University, India, 2004

Master of Science, Mechanical Engineering, Texas A&M University, College Station, Texas, 2007